© 2020. Published by The Company of Biologists Ltd | Development (2020) 147, dev192724. doi:10.1242/dev.192724

RESEARCH ARTICLE

β1 Integrin regulates convergent extension in mouse notogenesis, ensures notochord integrity and the morphogenesis of vertebrae and intervertebral discs

Shiny Shengzhen Guo[1,2], Tiffany Y. K. Au[1], Sarah Wynn[1], Attila Aszodi[3], Danny Chan[1], Reinhard Fässler[2] and Kathryn S. E. Cheah[1,*]

ABSTRACT

The notochord drives longitudinal growth of the body axis by convergent extension, a highly conserved developmental process that depends on non-canonical Wnt/planar cell polarity (PCP) signaling. However, the role of cell-matrix interactions mediated by integrins in the development of the notochord is unclear. We developed transgenic Cre mice, in which the β1 integrin gene (*Itgb1*) is ablated at E8.0 in the notochord only or in the notochord and tail bud. These *Itgb1* conditional mutants display misaligned, malformed vertebral bodies, hemi-vertebrae and truncated tails. From early somite stages, the notochord was interrupted and displaced in these mutants. Convergent extension of the notochord was impaired with defective cell movement. Treatment of E7.25 wild-type embryos with anti-β1 integrin blocking antibodies, to target node pit cells, disrupted asymmetric localization of VANGL2. Our study implicates pivotal roles of β1 integrin for the establishment of PCP and convergent extension of the developing notochord, its structural integrity and positioning, thereby ensuring development of the nucleus pulposus and the proper alignment of vertebral bodies and intervertebral discs. Failure of this control may contribute to human congenital spine malformations.

KEY WORDS: β1 integrin, Notochord, Convergent extension, Intervertebral discs, Hemi-vertebrae, Planar cell polarity

INTRODUCTION

The notochord is a rod-like midline structure of mesodermal origin that forms during gastrulation. Its formation and extension are among the earliest and most obvious events of axis development during embryogenesis (Jurand, 1974; Rossant and Tam, 2002; Stemple, 2005). In vertebrates, the notochord has two primary functions during embryonic development. Firstly, it serves as the axial skeleton of the embryo until vertebrae form. Secondly, it acts as a signaling center that induces the formation of floor plate in the neural tube (Jessell et al., 1989) and the differentiation of the ventral somatic derivatives into the sclerotome (Pourquie et al., 1993). Unlike in some lower vertebrates, such as lampreys, and some primitive fish, such as sturgeons, for which the notochord persists throughout life (Stemple, 2005; Corallo et al., 2015), the notochord in higher vertebrates is a transient structure that remodels during vertebral body formation leaving remnants in the intervertebral discs (IVDs) as nuclei pulposi (NP) (Stemple, 2005; Choi et al., 2008; McCann et al., 2012).

Time-lapse live imaging and cell lineage tracing of the mouse notochord revealed three distinct morphogenetic origins along the anterior-posterior (A-P) axis (Yamanaka et al., 2007). The anterior notochord arises through condensation of dispersed cells anterior to the forming node; the trunk notochord derives from cells of the ventral layer of the bilaminar node that move via convergent extension; and the tail notochord develops from peripheral node cells (Sulik et al., 1994; Kinder et al., 2001; Ezin et al., 2003; Yamanaka et al., 2007; Ukita et al., 2009). The convergent extension of the notochord is stimulated by mechanical forces exerted by the expanding amniotic cavity as the mouse embryo elongates along the A-P axis (Imuta et al., 2014). These forces were shown to trigger membrane accumulation of VANGL2 and, thereby, the planar cell polarity (PCP) pathway. Whether and how these forces, the accompanying convergent extension and subsequent remodeling of the notochord to form NP are regulated by cell-matrix interactions is not known.

Notochordal cells are surrounded by a sheath of extracellular matrix (ECM), which contains glycoproteins such as fibronectin (FN), collagens and proteoglycans (Gotz et al., 1995; Smits and Lefebvre, 2003). In *Sox5* and *Sox6* double knockout mice, the notochord lacks the ECM sheath, resulting in impaired cell survival, lateral displacement of notochord cells and absence of the NP (Smits and Lefebvre, 2003). A major component of the notochordal sheath is collagen II, secreted by notochordal cells. In mice lacking collagen II, the notochord is enlarged in diameter, but is not remodeled and remains as a rod-like structure until birth, resulting in the failure to develop an IVD and NP (Aszódi et al., 1998). These defects indicate that the notochordal sheath is key for the reorganization of the notochord and IVD development, and support the hypothesis that notochordal cell-ECM interactions are probably mediating mechanical forces required for notochord reorganization (Aszódi et al., 1998; Lawson and Harfe, 2015).

Integrins are α/β heterodimeric cell adhesion molecules that mediate the interactions of cells with ECM proteins including collagens, FN and proteoglycans (Hynes, 2002). They are bidirectional signaling molecules that are first activated from within a cell, then bind ligands and transduce biochemical and physical properties across the plasma membrane into cells (Sun et al., 2016). Genetic studies in *Xenopus*, zebrafish and mice

[1]School of Biomedical Sciences, LKS Faculty of Medicine, The University of Hong Kong, Pokfulam, Hong Kong SAR, China. [2]Max Planck Institute of Biochemistry, Department of Molecular Medicine, 82152 Martinsried, Germany. [3]Department of General, Trauma and Reconstructive Surgery, Munich University Hospital, Ludwig-Maximilians-University, Fraunhoferstraβe 20, 82152 Planegg-Martinsried, Germany.

*Author for correspondence (kathycheah@hku.hk)

S.S.G., 0000-0001-9899-7491; A.A., 0000-0003-3569-6557; D.C., 0000-0003-3824-5778; R.F., 0000-0002-0145-6937; K.S.E.C., 0000-0003-0802-8799

Handling Editor: James Briscoe
Received 18 May 2020; Accepted 1 October 2020

Development (2020) 147, dev192724. doi:10.1242/dev.192724

implicated FN, laminin (LN) and the α5 integrin in notochord development and elongation along the A-P axis (George et al., 1993; Parsons et al., 2002; Pulina et al., 2014; Trapani et al., 2017). The β1 integrin subunit associates with any of 12 α subunits, and thereby forms the largest subfamily of ECM-binding integrins. However, as the constitutive deletion of the *Itgb1* gene encoding β1 integrin leads to peri-implantation lethality (Fassler and Meyer, 1995; Stephens et al., 1995), the role of β1 integrin during notochord development has not yet been elucidated.

To investigate the role of β1 integrin in notochord morphogenesis, we developed a transgenic Cre recombinase deletor strain to inactivate *Itgb1* in the mouse notochord. Characterization of these mice demonstrated Cre activity either in the notochord alone or in the notochord and the tail bud. The resulting mutant mice (designated *Itgb1*$^{\Delta ND}$) developed notochordal and vertebral column defects that resembled those of α5 integrin- and FN-deficient mice. We also report that β1 integrin promotes convergent extension movements and the asymmetric accumulation of the core PCP component VANGL2 in the node pit cells. Our findings assign β1 integrin-mediated cell-matrix adhesion as a key function in notochord morphogenesis.

RESULTS

Abnormal NP and disorganized vertebral patterning in the absence of β1 integrin

In order to ablate *Itgb1* specifically in the notochord, we developed a notochord-specific Cre (*Foxa2mNE-Cre*) transgenic mouse, in which bicistronic Cre and *lacZ* expression is driven by the *Sox9* promoter and a minimal notochord enhancer element isolated from the *Foxa2* gene (Sasaki and Hogan, 1996) (Fig. S1A). The earliest transgene expression visualized by *lacZ* staining was at around embryonic day (E) 7.5 in the node, extending into the notochord or in both the notochord and tail bud at later stages (Fig. S1A, black arrows). In crosses of the *Foxa2mNE-Cre* with an EGFP Cre reporter strain (*zEG*) (Novak et al., 2000), EGFP expression was activated in the notochord as early as E8.0, albeit in a mosaic pattern (Fig. S1B, white arrows), and in crown cells from the peripheral node, but not in pit cells located in the node center (Fig. S1B, highlighted region).

Next, we analyzed the Cre activity by tracking the GFP signals in ∼400 *Foxa2mNE-Cre;zEG* embryos obtained from different male breeders. Three types of Cre activities were observed at E9.5 (Fig. S1C). Type I (50%) showed strong activity in the entire notochord and some activity in the tail bud from E9.5, which probably reflects the contribution of node cells to the tail bud (Cambray and Wilson, 2002). The remaining 50% of embryos exhibited two types of notochord-specific Cre activities: one is strong (Type II, 37%) and the other is weak (Type III, 13%) (Fig. S1D). Cre expression ceased around E14.5, and GFP+ notochord descendants were found in the NP at adult stages (Au et al., 2020), which is consistent with published reports demonstrating a notochordal origin of NP cells (Choi et al., 2008; McCann et al., 2012). Thus, we utilized this *Foxa2mNE-Cre* mouse line to study gene function in cells of the developing notochord.

Next, we crossed mice homozygous for the floxed *Itgb1* (*β1*$^{F/F}$) allele with heterozygous *Foxa2mNE-Cre* transgenic mice. The latter were used as controls in our study. Immunostaining revealed significant reduction of β1 integrin expression at E8.0 (∼1 somite) (Fig. 1A) in the developing notochord marked by brachyury (T). By the ∼23 somite stage (E9.5), β1 integrin expression was absent in mutant cells in notochordal segments displayed as Region-1 (Fig. 1B, Region-1), indicating that β1 integrin protein has a maximal lifetime of ∼1.5 days in the notochordal tissue. Consistent with a combination of mosaic Cre activity and the stability of β1 integrin, β1 integrin expression was still detected at variable levels in notochordal regions relative to the surrounding non-notochordal cells (Fig. 1B, Region-2 and Region-3). Detailed analysis of the trunk and tail notochord from three embryos at E9.5 showed variable mosaicism in mutants ranging from ∼16-30% (Fig. S2A, B). Cre activities at later embryonic stages (E11.5 and E12.5) were also tracked. Notably, only notochord and notochord-descendants were affected, not the surrounding SOX9+ cells at the level before the hindlimb bud (Fig. S3A,B). At relatively posterior regions, such as levels of the sacral and tail vertebrae, the expression of β1 integrin in the surrounding somatic regions was also slightly decreased compared with the control (Fig. S3C). Approximately half (54%, 111 out of 206) of *Itgb1*$^{\Delta ND}$ mice could be distinguished from their littermates at birth by short and distorted tails (Fig. 2A), which may be representative of the Type I Cre activity. The remaining 46% of *Itgb1*$^{\Delta ND}$ mutants had normal tails, which is in line with Type II and III Cre activities (Fig. S1D). *Itgb1*$^{\Delta ND}$ mutants were viable, fertile and had normal life spans.

At postnatal day (P) 20, control mice had straight tails. Vertebrae had similar morphology and sizes, and were connected via IVDs (Fig. 2Aa). In sharp contrast, the severely affected *Itgb1*$^{\Delta ND}$ mice resulted from Type-I Cre activity showed misaligned and malformed tail vertebrae (Fig. 2Ab). Some of the mutant tail vertebrae resembled hemi-vertebrae (Fig. 2-Ab′ and Ab ″), seen in a rare congenital spinal malformation in human, in which only one side of the vertebral body develops, resulting in deformation of the spine (Varras and Akrivis, 2010). In some regions, the entire skeletal elements were absent (Fig. 2Ab, black arrow).

Histological analysis showed that each IVD in the control mice contained an NP in the core of the IVD (Fig. 2B, black arrows) sandwiched by two cartilaginous end-plates and surrounded by an inner and an outer annulus fibrosus. In the *Itgb1*$^{\Delta ND}$ mutants, the NP were either smaller or absent from IVDs (Fig. 2B, red arrows). Detailed histological analysis at every fifth section at P10 revealed that the NP were missing at random intervals along the spine from thoracic level to posterior tail vertebrae (Table S1; Fig. S4). In addition to the NP absence observed at the postnatal stage, the notochord remnants at E12.5 were also revealed to be abnormally displaced from the center of the intervertebral mesenchyme (IM), compared with the centrally localized notochord remnants in the control embryo (Fig. S5, red arrows). These two mutant phenotypes suggest that a lack of β1 integrin specifically in the notochord results in abnormal NP formation, defective IVDs and curved upper spine (e.g. in the thoracic level), and that a lack of β1 integrin in the notochord and tail bud results in misshapen vertebrae in the tail.

Discontinuous and displaced notochord in *Itgb1*$^{\Delta ND}$ mice

To investigate the cause of NP loss within the IVD, we assessed notochord development at different stages of embryogenesis (E8.0 to E10.5, Fig. 3A). In control embryos, the notochord marked by *T* was a continuous midline structure from the anterior to almost the tip of the tail. The notochord in *Itgb1*$^{\Delta ND}$ mice was interrupted at different locations along the A-P axis, which was evident as early as the 3-4 somite stage (Fig. 3A; Fig. S7A, red arrows). This discontinuity in *Itgb1*$^{\Delta ND}$ mice was confirmed by whole-mount *in situ* hybridization (WISH) with two additional notochord markers, *Shh* and *Noto* (Fig. S6A). Larger interruptions were found in the posterior regions and at later stages, such as E9.5 (Fig. 3A, red arrows).

Development (2020) 147, dev192724. doi:10.1242/dev.192724

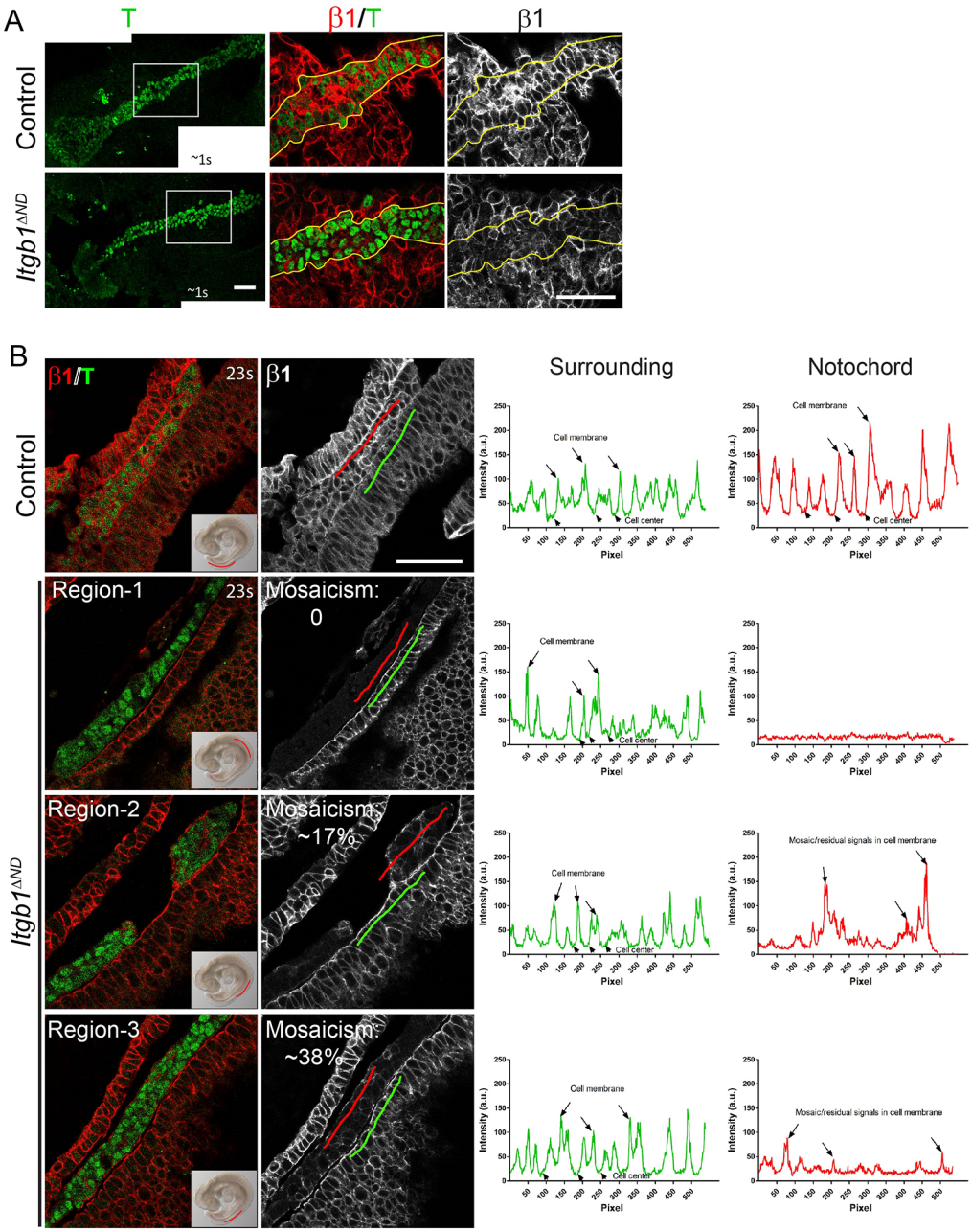

Fig. 1. Mosaic loss of β1 integrin in the mutant notochord. (A,B) Immunostaining against β1 integrin (red) and notochord marked by T (green) in whole embryos at E8.0 (A) and in sagittal sections at E9.5 (B). (B) The regions analyzed were indicated with a red line along the E9.5 embryo in the inset for each image. Intensity of β1 integrin was analyzed via profile analysis and expressed as arbitrary unit (a.u.). Notochord region, red lines; surrounding neural tube, green lines. The mosaicism counted (%) was labeled for each region. Intensity of β1 integrin is high in the cell membranes (long arrows) and low in the cell center (short arrows). β1 Integrin signals at different notochordal levels in the same mutant showed different intensities, reflecting different degrees of mosaicism. Scale bars: 50 µm.

In order to distinguish whether the discontinuous *T* expression is due to cell fate change or defective structural integrity, we sectioned E8.25 embryos after WISH (Fig. S6B) and E9.5 embryos for immunostaining (Fig. S6C). Whereas control E8.25 embryos displayed intense *T* RNA signals below the folding neural tube, the *Itgb1*$^{\Delta ND}$ embryos lacked *T* expression in the interrupted region (Fig. S6B). At E9.5, the notochord structure from control embryos showed DAPI- and T-positive nuclei, whereas *Itgb1*$^{\Delta ND}$ embryos lacked DAPI-positive notochordal cells beneath the floor plate in some regions (Fig. S6C). Despite the interruptions in the *Itgb1*$^{\Delta ND}$ notochord structure, the patterning of the floor plate and the neural tube were unaffected, as reflected by the expression patterns of molecular markers such as PAX6, PAX7 and NKX2.2 (Fig. S6D; Yamada et al., 1991; Roelink et al., 1995; Ericson et al., 1997; Briscoe et al., 1999, 2000).

Notochord-derived signaling is also known to induce the differentiation of the ventral somatic derivatives into the sclerotome (Pourquie et al., 1993). Thus, we also examined the somite differentiation from E8.5 to E10.5 using WISH for *Uncx4.1* (*Uncx*) and *Pax1*. Consistent with the different Cre activities observed, somite formation was normal up to E9.5, but *Pax1* expression was interrupted in the tail somites of some mutant embryos at E10.5 (Fig. S7A-C), which could be caused by the activity of Type I Cre. This observation correlates with an obvious tail abnormality in the mutants from E12.5 (Fig. S8).

To understand the developmental basis of the NP phenotype, we focused our further analyses on early embryonic stages when expression of Cre was restricted to the notochord. The notochord is initially formed as a plate of cells embedded inside the dorsal gut endoderm. As soon as the cells fold off from the endoderm roof, they form a cylindrical rod-like structure, called the definitive notochord (Jurand, 1974; Sulik et al., 1994; reviewed by Balmer et al., 2016). Later, as the surrounding mesenchymal cells penetrate the space between the floor plate and the notochord, the notochord

Development (2020) 147, dev192724. doi:10.1242/dev.192724

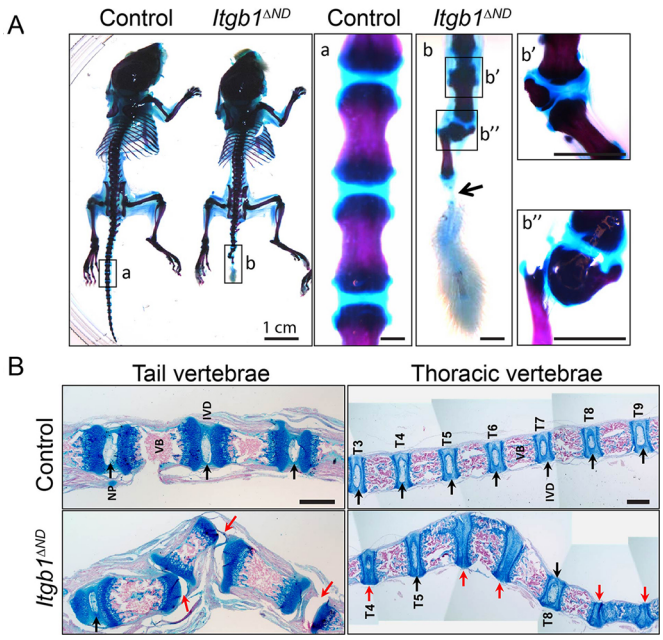

Fig. 2. Loss of β1 integrin in notochord led to abnormal NP formation, defective IVDs and disorganized vertebral patterning of the spine. (A) The gross morphology of the skeletons of control and *Itgb1*$^{\Delta ND}$ mutant mice was analyzed at P20 via skeletal preparations (n=4 for each genotype). (Aa-Ab) More details of the tail region. Arrow in A2 indicates the missing skeletons. (Ab′-Ab″) The disorganized vertebrae in the mutant, which resemble the hemi-vertebrae, is highlighted. (B) Histological analysis of spines showing morphology of the IVD and NP at P10. Black arrows indicate the normal NPs. Red arrows indicate the abnormal NPs. IVD, intervertebral disc; Tn, level of the thoracic vertebrae; VB, vertebral body. Scale bars: 0.5 mm (unless stated otherwise).

separates from the neural tube. At the more anterior region of control E9.0 embryos (~16-17 somites), the notochord adhered to the midline structures on both sides, the overlying neural tube and the underlying foregut (level Ba in Fig. 3B). Slightly more posteriorly, the notochord had detached from the endoderm but still adhered to the ventral side of the neural tube (level Bb in Fig. 3B), leaving the notochord at the center of the dorsal-ventral (D-V) midline axis (Fig. 3B, dotted lines). In *Itgb1*$^{\Delta ND}$ embryos, the notochord had separated from the neural tube and displayed prolonged contact with the endoderm, resulting in an abnormally large, acellular space between the neural tube and the notochord and, hence, displacement of the notochord from the D-V midline axis (Fig. 3B).

In control E9.5 embryos, the rod-like notochord structure was located at the left-right (L-R) midline axis between the neural tube and foregut endoderm, whereas in *Itgb1*$^{\Delta ND}$ embryos the notochord was displaced to the lateral side of the neural tube, away from the L-R midline axis (Fig. 3C). In line with these findings, *WISH* analysis revealed that *T* signals were displaced in some regions from the midline axis (yellow arrows in Fig. 3A), which possibly resulted in the displaced notochord remnants observed at E12.5 (Fig. S3C, asterisk; Fig. S5, red arrows). These data suggest that the absence of β1 integrin in *Itgb1*$^{\Delta ND}$ embryos leads to cell loss in the notochord. The consequential interruptions and defective structural integrity and alignment in the notochord affect its positioning.

Abnormal matrix deposition around the *Itgb1*$^{\Delta ND}$ notochord

Integrin-mediated cell-ECM adhesion signaling supports cell survival (Frisch and Ruoslahti, 1997) and cell proliferation (Legate et al., 2006). As the *Itgb1*$^{\Delta ND}$ embryos consistently displayed notochord defects with interruptions (~70%) (Table S2), we next examined whether the cell loss was due to mesoderm deficiency or impaired cell proliferation or survival. EdU (E8.5, Fig. 4A) and BrdU (E9.5, Fig. 4D) staining showed that at E8.5 ~30% (Fig. 4B) and at E9.5 ~22% (Fig. 4G) of the cells within the notochordal plate incorporated the DNA dyes in both control and *Itgb1*$^{\Delta ND}$ embryos. In line with a previous report (Bellomo et al., 1996), numerous cells surrounding the notochord and in the primitive streak were also actively proliferating in control and *Itgb1*$^{\Delta ND}$ embryos (Fig. 4A).

To test whether the notochord interruptions are due to increased apoptosis, we performed whole-mount immunostaining for active caspase 3 (actCas3) at E8.5. In control and *Itgb1*$^{\Delta ND}$ embryos, scattered actCas3 signals were detected in the mesenchyme surrounding the notochord (Fig. 4Ca′,Ca″,Cb′,Cb″, yellow arrows), but not within the notochord or in regions with gaps (Fig. 4Cb′,Cb″, white arrows). Staining in the posterior region of E9.5 *Itgb1*$^{\Delta ND}$ embryos (Fig. 4E), in which the defective notochord phenotype was particularly prominent (Fig. 4F), revealed very few actCas3-positive cells in the notochord region, which was also the case in control embryos (Fig. 4H). However, *Itgb1*$^{\Delta ND}$ embryos had occasional aggregates of T-positive cells at the tip of interrupted segments (Fig. 4I, oval outline).

FN is the major ligand of α5β1 integrin and a major component of the notochordal sheath (Gotz et al., 1995; Smits and Lefebvre, 2003). In control embryos, FN was strongly enriched in the sheath surrounding the notochord; however, it was significantly decreased in the notochord sheath of *Itgb1*$^{\Delta ND}$ embryos with notochord displacement, suggesting that β1 integrin loss is the reason for the weakened/reduced FN sheath formation (Fig. 4J). Moreover, some *Itgb1*$^{\Delta ND}$ embryos displayed an acellular ‘ghost’ notochord surrounded by an LN-containing sheath (Fig. 4K).

Impaired convergent extension movement and wide notochord in *Itgb1*$^{\Delta ND}$ embryos

In chordate notogenesis, convergent extension is one of the major processes by which the cells converge towards the midline, driving the elongation of the notochord along the A-P axis (Ezin et al., 2003; Sausedo and Schoenwolf, 1994; Yamanaka et al., 2007). During the lengthening of the node along the A-P axis, cells in the axial midline intercalate along the medial-lateral (M-L) axis, resulting in a notochordal plate consisting of two adjacent rows of cells (Yamanaka et al., 2007). To determine whether impaired convergent extension contributes to the notochordal defects of *Itgb1*$^{\Delta ND}$ embryos, we compared cellular intercalation and the length/width ratio (LWR) of the developing notochord of control and *Itgb1*$^{\Delta ND}$ embryos. In controls, T immunostaining showed the notochordal plate in the midline containing two rows of cells up to the node level (Fig. 5A, white lines before the node). By contrast, in stage-matched *Itgb1*$^{\Delta ND}$ embryos, the notochordal plates were wider, contained more rows of cells (Fig. 5A, highlighted by yellow lines), had more cells per somite (Fig. 5B, P<0.05) and a reduced LWR within the somite region (~25% lower than controls; Fig. 5C, P<0.005). This correlates with the obviously wider notochord at E9.5 (Figs 3C, 5D, P<0.0001).

In order to understand the cellular basis of the wider notochordal plate, we performed time-lapse live imaging of the node region using the EGFP reporter mouse line (*zEG*) (Novak et al., 2000). Embryos with 1-2 somites were cultured and imaged overnight for ~17 h (Fig. S9A). At the end of overnight culture, the embryos had usually developed into stages with 8-9 somites, depending on the starting age of the embryo (Fig. S9A). To exclude any effects introduced by photo-toxicity during overnight imaging, the embryos

Development (2020) 147, dev192724. doi:10.1242/dev.192724

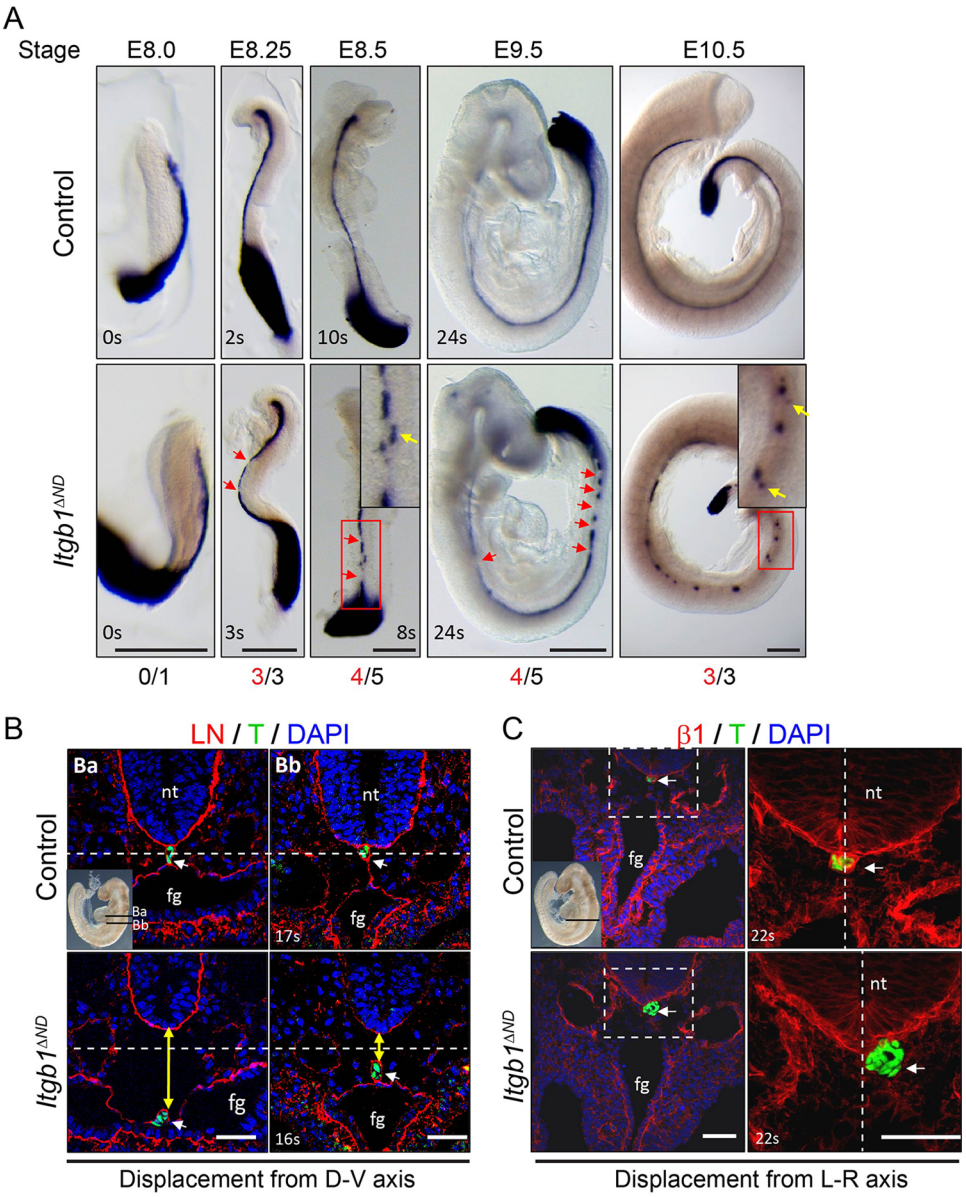

Fig. 3. Deficiency of β1 integrin led to interrupted and displaced notochord. (A) WISH using *T* riboprobe in embryos from different embryonic stages. Red arrows, interrupted notochord. Yellow arrows, displaced notochord. Numbers under the panels indicate embryo numbers (black) and embryo numbers with defects (red). (B,C) Immunostaining against T (green) and LN (red) (B) or β1 integrin (red) (C), and DAPI (blue) on cross-sections showing the displacement of notochord from both t he D-V (B) and L-R axes (C) in the mutants. Ba and Bb in inset show the levels of the section in main panels. White arrows, notochord. Yellow double-edged arrows show the space between nt and the fg. fg, foregut; nt, neural tube. Scale bars: 0.5 mm in A; 50 µm in B.

were dissected to check their morphology and only healthy ones were selected for further analysis. In an E8.0 embryo with ∼1 somite, the anterior notochordal plate had already formed. Single cell tracking in the node peripheral region with crown cells, in which the most active morphogenesis occurs (Fig. S9C, white arrows), revealed that the convergent movement of node cells to the midline is coupled with directionally persistent movement in an A-P direction along the midline in the control embryos (Fig. 5E, upper panel; Movie 1). In contrast, in mutant embryos, the node cells displayed a tumbling behavior near their original positions during the first 3 h (Fig. 5E, ∼0-200 min, lower panel; Movie 2). Ultimately, movement towards the posterior did occur, albeit with lower directionalities (Fig. 5F, $P<0.0005$). Quantitative analysis revealed no significant difference in velocities and accumulated migrating distances between control and β1 integrin-deficient node cells (Fig. 5G,H). However, owing to the reduced directionality, mutant node cells traveled less far in Euclidean distances (Fig. 5I, $P<0.0004$). Thus, the compromised notochord convergent extension observed in the mutants is due to reduced directional persistence of cell movement upon reduced β1 integrin expression (Fig. S10).

To assess the impact of loss of β1 integrin on intercellular adhesion of the mouse notochord, we analyzed N-cadherin expression in the mutants with defective convergent extension. Compared with the control notochord, the N-cadherin signal was enhanced in the mutant notochord from anterior to posterior at E8.5 (Fig. 6A,C, $P<0.0001$) and at E9.5 (Fig. 6B,C, $P<0.0001$).

Wnt/PCP signaling is a key conserved mechanism coordinating polarized cell behaviors (Gray et al., 2011; Yang and Mlodzik, 2015). In vertebrates such as zebrafish, it regulates convergent extension along the embryonic A-P axis (Heisenberg et al., 2000; Park and Moon, 2002; Kilian et al., 2003), and in *Xenopus*, through the assembly of the FN matrix (Dzamba et al., 2009). In mouse, the pit cells in the center of the node establish PCP as early as E7.5 (Hashimoto et al., 2010; Mahaffey et al., 2013) and show clear asymmetric VANGL2 localization at E8.25 (Song et al., 2010; Mahaffey et al., 2013). In line with no *Foxa2mNE-Cre* activity in pit cells using the current transgenic Cre tool (Fig.S1B), we detected asymmetric VANGL2 localization in both control and *Itgb1*$^{\Delta ND}$ mutants (Fig. S11A,B), suggesting that PCP establishment in the central node is a cell-autonomous behavior,

Development (2020) 147, dev192724. doi:10.1242/dev.192724

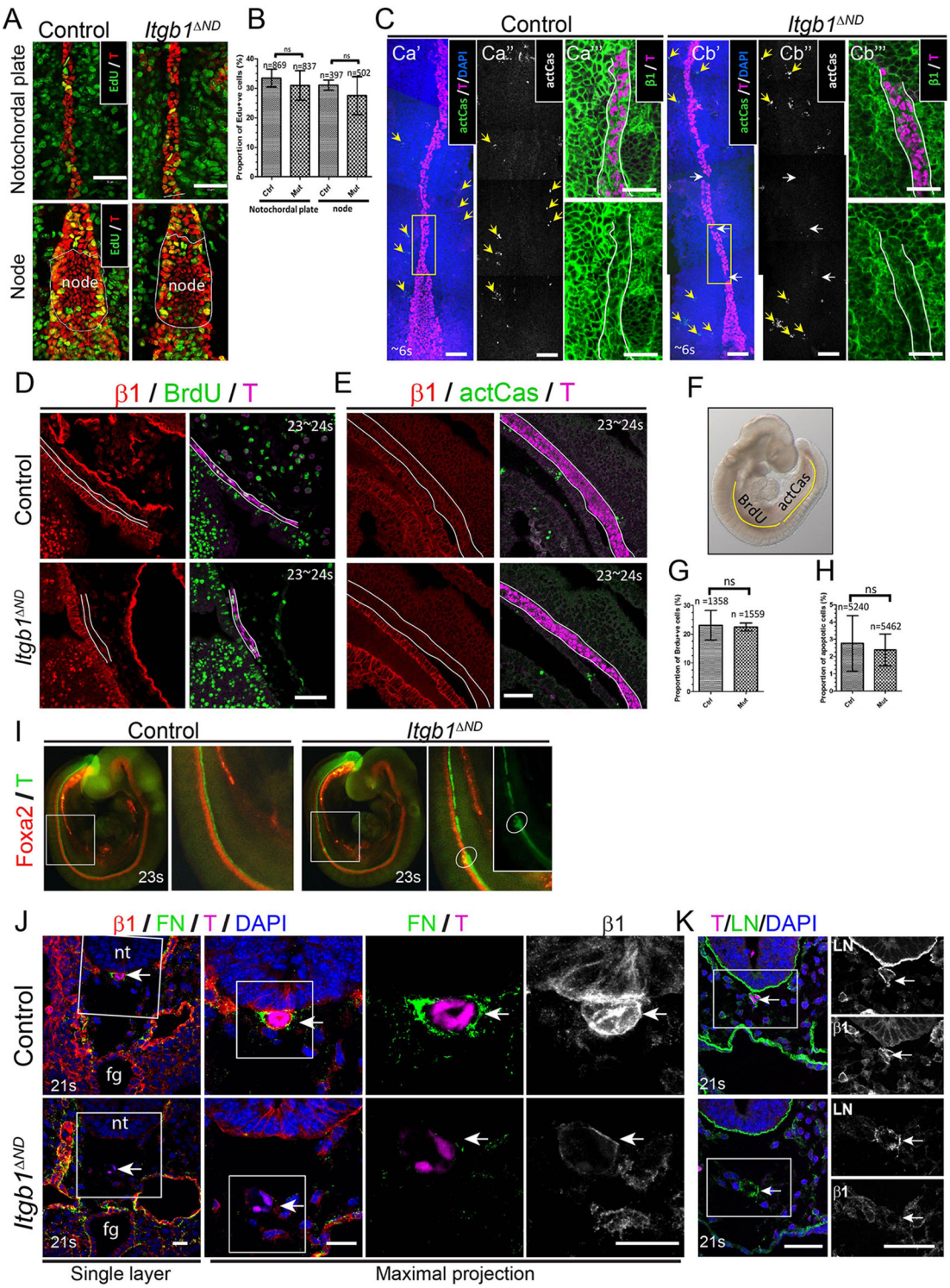

Fig. 4. See next page for legend.

which is not affected by the *Itgb1* deletion in the surrounding crown cells.

In order to determine whether β1 integrin is required for PCP establishment, we cultured wild-type embryos from E7.25 to E8.25 (Fig. S12A) in the presence of control or β1 integrin functional blocking antibodies. At the end of culture, the embryo overall morphology and body length between two groups were similar (Fig. S12A,B). As shown in Fig. 7A, embryos cultured overnight with the isotype-control antibody displayed clear asymmetric localization of VANGL2 in the center of the node in which the pit cells are localized. In sharp contrast, the number of cells showing asymmetric VANGL2 distribution was significantly reduced in pit cells of embryos cultured with β1 integrin functional blocking antibodies (Fig. 7A,B, arrows indicate cells with asymmetric VANGL2 and asterisks indicate cells without clear VANGL2 asymmetry). The few cells with normal, asymmetric VANGL2

Development (2020) 147, dev192724. doi:10.1242/dev.192724

Fig. 4. β1 Integrin is not required for notochord cell proliferation and survival but is required for FN matrix deposition surrounding the notochord. (A,B) Cell proliferation assay analyzed via EdU incorporation in Control (Ctrl) and *Itgb1*$^{\Delta ND}$ mutant embryos (Mut) at E8.5 showing EdU (green) and T (red). Both the node and the notochordal plate regions are quantified (B). Data are mean±s.d. (n=4 for each genotype, unpaired two-tailed Student's t-test). (C) Cell apoptosis analyzed via active caspase 3 (actCas) staining. (Ca′,Cb′) Immunostaining against T (magenta), actCas (green) and DAPI on whole embryos at E8.5 (n=3 for each genotype). (Ca″,Cb″) Grey channels for actCas signals. Yellow arrows show scattered actCas signals outside notochord region. White arrows show interrupted gaps in mutant notochord. (Ca‴,Cb‴) The corresponding β1 integrin expression is shown in green. (D,G) Cell proliferation assay analyzed via BrdU incorporation (D, green) and quantified in G. Data are mean±s.d. at E9.5 (n=3 for each genotype, unpaired two-tailed Student's t-test). (E,H) Cell apoptosis analyzed via actCas (green) immunofluorescence (E) and quantified in H. Data are mean±s.d. at E9.5 (n=5 for each genotype, unpaired two-tailed Student's t-test). Embryo stage is indicated with somite numbers. (F) The regions used for either BrdU incorporation or actCas analysis are illustrated. (I) Whole-mount immunostaining against Foxa2 (red) and T (green). Notochordal cells were clumped at the site adjacent to the broken points (highlighted with oval frames). (J,K) Immunostaining of the notochord sheath against FN or LN [n=5 for control and n=4/7 for mutants in which 4 out of 7 (57%) showed reduced FN assembly]. These four embryos showed obvious defects with either D-V, L-R deviation or interrupted notochord. Arrows indicate notochord. Panels on right show magnification of boxed areas in left panels. ns: no significance (unpaired two-tailed Student's t-test). fg, foregut; nt, neural tube. Scale bars: 50 µm for A,C,D,E,K; 20 µm for J.

distribution (Fig. S12C,D) were likely not fully blocked with the β1 integrin antibody. Altogether, these data point to a role of β1 integrin signaling in the establishment of PCP in the pit cells of the node.

Impaired cell-matrix interactions in the absence of β1 integrin expression

The notochord of an E9.5 mouse embryo is a tiny structure with ∼1500 cells. Notochordal cells isolated via cell sorting do not proliferate and cannot be maintained *in vitro* under normal culture condition (S.S.G. and K.S.E.C., unpublished). To obtain enough cells for *in vitro* analysis, we immortalized notochordal cells via retroviral transduction with the SV40 large T antigen. Antibody staining with two notochord markers, Foxa2 and T, suggested that notochordal characteristics were maintained in the immortalized cells (Fig. S13A, upper panel). Expression profile analysis of integrins in the notochordal cells show that α5β1 (FN receptor) is the most abundant integrin, followed by the less abundant αvβ3 [vitronectin (VN) receptor] and α6β1 (LN receptor), and low collagen receptor expression (α1β1) (Fig. S13C).

To test whether cell-matrix interactions were changed once β1 integrin expression was lost, we deleted *Itgb1* using the CRISPR/Cas9 system. Gene deletion was verified by immunostaining (Fig. S13B), sequencing the frame shift (Fig. S13D) and western blot (Fig. 8E,F). Although cells lacking β1 integrin (β1-KO) are smaller than parental control cells, notochordal identity was maintained, as defined by Foxa2 and T expression (Fig. S13A, lower panel).

Next, we performed cell adhesion assays on different substrates (Fig. 8A) and found that β1-KO cells failed to adhere to collagen I and LN, and to a lesser extent to FN and VN when compared with control cells. The reduced adhesion of β1-KO cells on FN was associated with an inability to spread (Fig. 8B) and to migrate in scratch assays (Fig. 8C). Detailed cell tracking analysis revealed that migrating distance, speed and directionality were impaired in β1-KO cells (Fig. 8D). The pronounced spreading and migration defects of β1-KO cells were accompanied by reduced GTP-Rac1 and GTP-Cdc42 activities (Fig. 8E). Moreover, consistent with the observation *in vivo*, N-cadherin expression level was also upregulated in the β1-KO cells (Fig. 8F).

DISCUSSION

Although a key characteristic of the notochord is its midline position, it is unclear to what degree deviation from this feature contributes to its functional attributes and influences the overall patterning and alignment of the vertebral bodies and IVDs of the spine. Further, the role of cell-matrix interactions mediated by β1 integrin, the core subunit of the largest subfamily of ECM-binding integrins, in notochord induction and morphogenesis, and notochord integrity and signaling function, is unknown because notochord-specific manipulations of the gene have been lacking. In this study, we employed a notochord-specific enhancer from the mouse *Foxa2* gene to drive Cre recombinase-mediated ablation of β1 integrin expression specifically in notochordal cells at early somite stages. We report that loss of β1 integrin in the *Itgb1*$^{\Delta ND}$ mutants impacts the structural integrity and midline positioning of the notochord, which in turn affects the proper development of vertebrae and IVDs in the spine. Our study shows that these defects arise because convergent extension of the notochord during its morphogenesis and its activity in vertebral body patterning are impaired.

β1 Integrin ensures structural integrity and midline position of the notochord

Cell lineage tracing studies have suggested that all cells of the mouse NP, from tissue formation through to skeletal maturity, are of notochord origin (Choi et al., 2008; McCann et al., 2012). A striking abnormality observed in the *Itgb1*$^{\Delta ND}$ mutants is the interruption of the notochord at multiple locations along the A-P axis, displacement from the midline axis and the presence of notochordal sheath segments devoid of cells. These abnormalities correlate with absence of NP in the IVD at postnatal stages and are consistent with this concept of the developmental origin and contribution of notochordal cells to the mature NP.

As *Foxa2mNE-Cre* expression commences at ∼E7.5-8.0, a stage at which the node structure has already matured (Mahaffey et al., 2013), and the half-life of the β1 integrin protein exceeds 24 h (Brakebusch et al., 2000), *Foxa2mNE-Cre* effectively ablates β1 integrin function in the notochord from ∼E8.5. Therefore, we can exclude defective development and morphogenesis of the node as cause for the notochord displacement from the midline axis. Our experiments also ruled out cell loss by apoptosis and/or reduced cell proliferation as the cause of the fragmented and dislocated notochord in *Itgb1*$^{\Delta ND}$ embryos.

Depletion of α5 and αV integrins in zebrafish results in a curled notochord that detaches from the paraxial mesoderm during trunk elongation (Dray et al., 2013). Constitutive deletion of the *FN* (*FN1*) gene in mice results in impaired mesoderm development and absence of the notochord (George et al., 1993). However, although mesoderm development in *Itgb1*$^{\Delta ND}$ embryos initiated normally, we noted reduced deposition of FN around the mutant notochord. As FN is assembled by α5β1 integrins into a stable and biologically active fibrillar structure, the absence of α5β1 integrins in *Itgb1*$^{\Delta ND}$ notochordal cells could contribute to the reduced FN in the notochordal ECM sheath marked by LN.

Mechanical forces exerted by the expanding amniotic cavity during mouse embryo elongation along the A-P axis have been shown to drive convergent extension of the mouse notochord (Imuta et al., 2014). Our findings suggest that notochord integrity and midline position depend on normal β1 integrin signaling, which

Development (2020) 147, dev192724. doi:10.1242/dev.192724

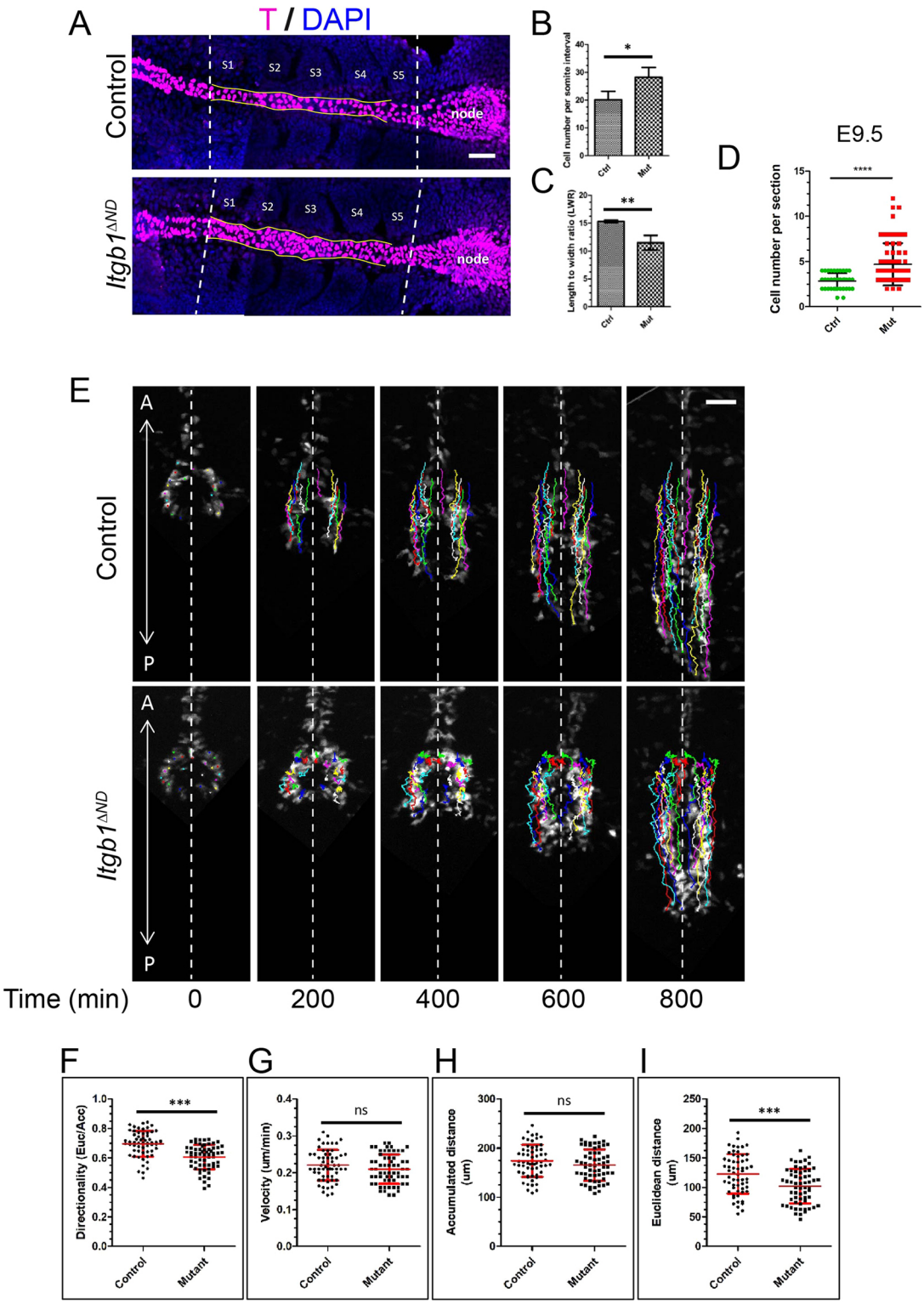

Fig. 5. Deficiency of β1 integrin resulted in impaired convergent extension with a wider notochord. (A) Immunostaining against T (magenta) and DAPI (blue) on whole embryos with ∼5-7 somites. The notochordal plate region was outlined with free-hand yellow lines. Somite identifications were indicated as s1 to s5. (B,C) Cell number counted (B) and the length:width ratio (LWR) measured (C) along the notochordal plate within the somite region in between the white dotted lines in A. Data are mean±s.d. from five pairs of control and mutant. **P*<0.05, ***P*<0.005 (unpaired two-tailed Student's *t*-test). (D) Quantification of the cell numbers per cross-section from E9.5 embryos. Around 6-8 sections were counted for each embryo (embryo number analyzed: *n*=5 for control and *n*=8 for mutant). *****P*<0.0001 (unpaired two-tailed Student's *t*-test). Refer to Fig. 2C for representative image. (E) Representative snapshot images of time-lapse movies from one experiment (*n*=3 for each genotype). Time points shown are at every 200 min. Cells used for cell movement tracking are highlighted with color dots. The corresponding tracking trajectories are merged to the images. A-P, anterior-posterior. (F-I) Plot of the statistical data on the node cell moving behaviors from three repeats (*n*=3 for each genotype), showing directionalities (F), velocities (G), accumulated (H) and Euclidean (I) distances. Cell numbers included in the plots are 59 for control and 61 for mutant group. Data are mean±s.d. ****P*<0.0005 (unpaired two-tailed Student's *t*-test). ns: no significance. Scale bars: 100 µm.

Development (2020) 147, dev192724. doi:10.1242/dev.192724

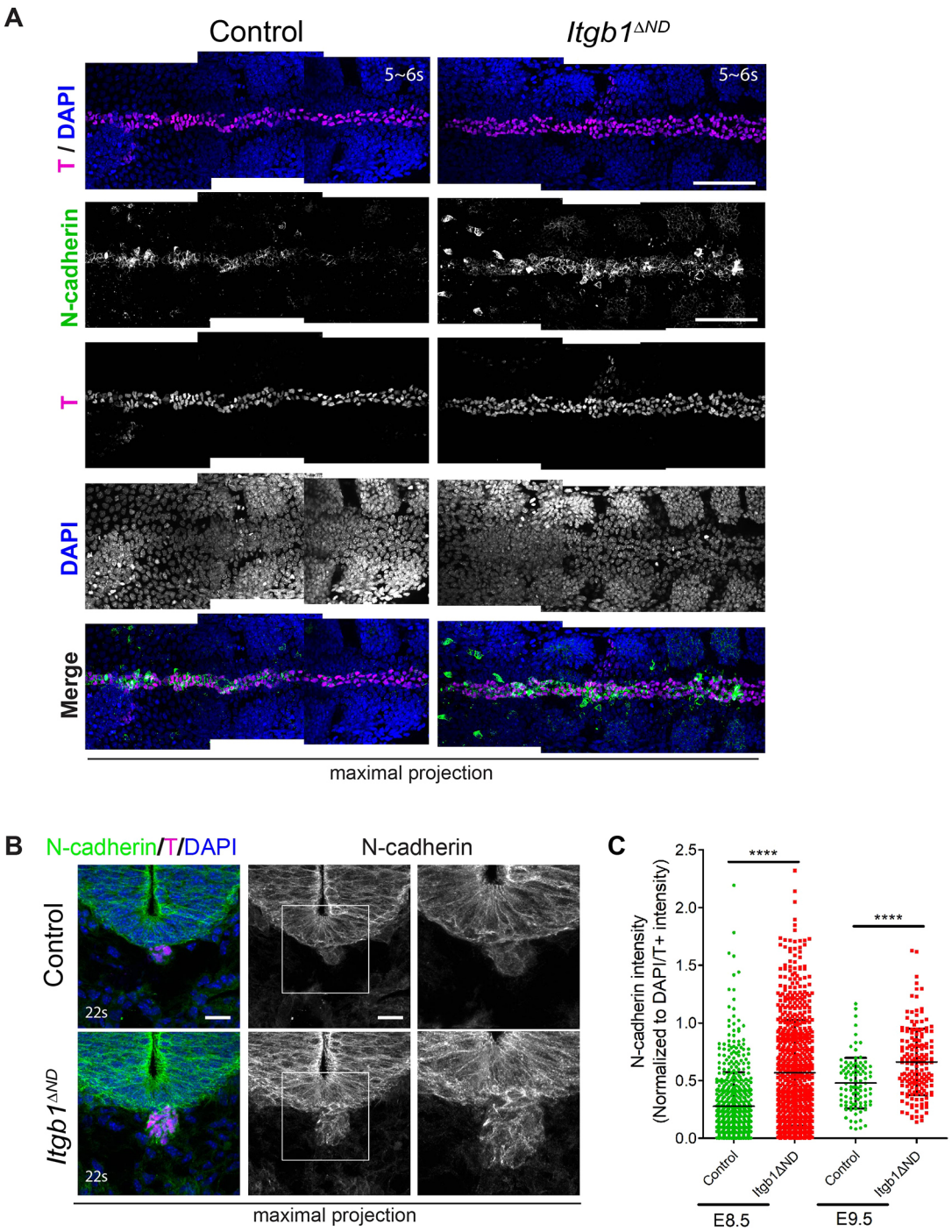

Fig. 6. Enhanced intercellular adhesions in the *Itgb1*$^{\Delta ND}$ mutants. (A) Whole-mount immunostaining against T (magenta), N-cadherin (green) and DAPI (blue) on embryos with ~5-6 somites. (B) Immunostaining against T (magenta), N-cadherin (green) and DAPI (blue) on cross-sections from E9.5 embryos. Right panels show magnification of boxed areas. (C) Statistical analysis of the N-cadherin intensities from three stage-matched embryo pairs at both stages. Cell numbers measured: 543 (control) and 709 (mutant) at E8.5; 98 (control) and 167 (mutant) at E9.5. Data are mean±s.d. ****P<0.0001 (unpaired two-tailed Student's t-test). The quantified N-cadherin intensities were normalized to the DAPI/T+ signals. Scale bars: 100 µm for A; 20 µm for B.

mediates mechanical coupling within the notochord tissue itself, rather than on the node geometry (Pulina et al., 2014). It is possible that the loss of β1 integrin in our mutants changed the structural composition of the notochord sheath, thereby affecting cell-matrix interaction and cell-cell adhesion, and altering the inter-tissue mechanical coupling between the notochord and the paraxial mesoderm. The defective integrin-mediated connection between notochord and peri-notochord tissue would render the notochord unable to withstand the mechanical forces generated during elongation, leading to fragmentation and the displaced midline structure.

Loss of β1 integrin impairs convergent extension leading to notochord widening

Although deficiency in ECM composition of the notochordal sheath could contribute to the interruptions and displacement of the

Development (2020) 147, dev192724. doi:10.1242/dev.192724

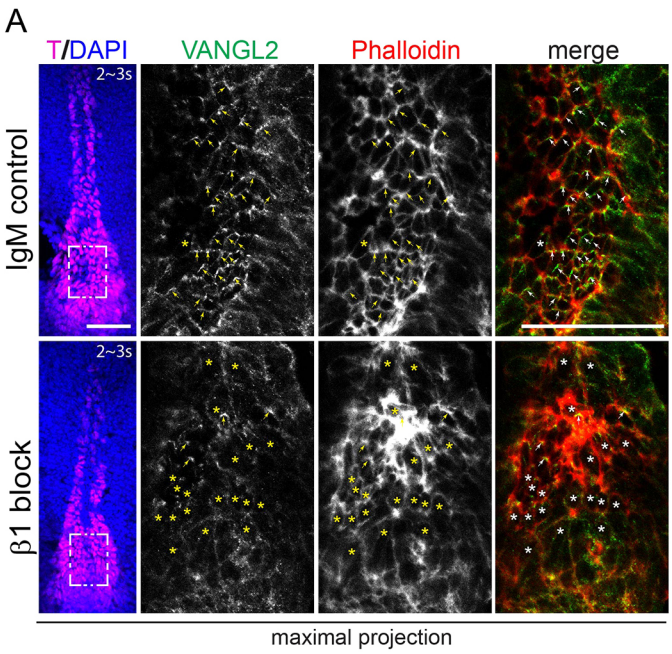

Fig. 7. Reduced asymmetric VANGL2 localization in the node when β1 integrin function is blocked. (A) Whole-embryo staining against T (magenta), VANGL2 (green), Phalloidin (red) and DAPI (blue). VANGL2 localization in the node center were shown in magnifications of boxed areas (right). Arrows show cells with asymmetric VANGL2 – note this pattern was much reduced in the blocking group. Asterisks show cells without clear VANGL2 asymmetry. (B) Reduced percentage of cells with asymmetric VANGL2 distribution. Data are mean±s.d. from three pairs of control (IgM) and β1 blocking group. $^{**}P<0.005$ (unpaired two-tailed Student's *t*-test). Scale bars: 50 µm.

notochord in *Itgb1*$^{\Delta ND}$ mutants, it is interesting that FN deficiency in the ascidian *Ciona* does not interfere with the development of a sheath surrounding the notochord, but profoundly affects intercalation and migration of notochordal cells and therefore convergent extension (Segade et al., 2016). Our experiments provide strong evidence that reduced directional persistence of the movement of notochordal cells lacking β1 integrin account, at least in part, for the defective notochordal convergent extension, midline positioning and acellular interruptions observed in *Itgb1*$^{\Delta ND}$ mice. The defective cell movement could be caused by impaired cell-cell or cell-matrix adhesion and/or altered biomechanical properties of the notochord and its sheath. In *Xenopus*, inhibition of β1 integrin function alters C-cadherin-mediated cell adhesion, affecting cell intercalation and inhibiting convergent extension and axial elongation of gastrulating embryos (Marsden and DeSimone, 2003). The abnormally high intercellular expression of N-cadherin observed in the *Itgb1*$^{\Delta ND}$ mutants and in the β1-KO notochordal cells suggests imbalance of cell-cell and/or cell-matrix adhesions between notochordal cells and the ECM sheath, contributing to the defective convergent extension.

β1 Integrin regulates PCP induction in the node

The PCP pathway has been shown to be involved in the assembly of ECM proteins such as FN in *Xenopus* gastrulation (Goto et al., 2005). The importance of the PCP pathway for notochord development was illustrated in embryos lacking the core PCP pathway genes *Vangl2* (*lp/lp* mice) and *Ptk7*, in which the notochordal plate widened (Yen et al., 2009; Mahaffey et al., 2013; Imuta et al., 2014). PCP is established in the pit cells of the node, which give rise to the anterior notochord/notochordal plate (Hashimoto et al., 2010; Song et al., 2010). However, VANGL2 was properly localized in the node of *Itgb1*$^{\Delta ND}$ embryos. This result is probably because the notochord-specific *Cre* line used in our study is not active in pit cells and does not prevent β1 integrin expression until ∼E8.0-E8.5, which is after the node has matured and PCP is established (Mahaffey et al., 2013). It is also of note that *Vangl1* but not *Vangl2* is expressed in the developing notochord (Torban et al., 2008) and *Vangl1* mutants do not display an embryonic PCP phenotype (Torban et al., 2008; Song et al., 2010).

To circumvent the lack of Cre activity in the pit cells, wild-type embryos were treated with anti-β1 integrin blocking antibodies, which are in IgM isotype. Fc domains present in both IgG and IgM are known to mediate antibody transmission from mother to young in mammals via the Fc receptor expressed in the surface of the embryo yolk sac (Roberts et al., 1990; Kim et al., 2009; Merad and Wild, 1992). Although we cannot discount possible differences between the transmission of the functional blocking antibodies and the corresponding IgM isotype control, the results of the antibody blocking experiments strongly suggest that β1 integrin is important for the early establishment of PCP in the node, which could impact on the developing notochord.

It is possible that the convergent extension defect and the altered migration of notochordal plate cells observed in 5- to 7-somite-stage mutant embryos may not be caused by a VANGL-mediated PCP defect. Such a scenario would be consistent with other examples, in which the relationship between PCP and convergent extension is not definitive (Tada and Heisenberg, 2012; Sutherland et al., 2020). Later in notochord development, β1 integrin may work with different PCP components to regulate convergent extension (Imuta et al., 2014; Sutherland et al., 2020). In *Itgb1*$^{\Delta ND}$ mutants, convergent extension is impaired because this role is abrogated and/or additional external mechanical forces contribute. Further studies are needed to distinguish between these possibilities and determine whether β1 integrin itself and/or the downstream signaling effectors indeed interact with components of the PCP pathway to regulate mouse notochord convergent extension, for example, by using a mouse line that expresses Cre in the pit cells and works before node formation.

Notochord fragmentation impairs IVD and vertebral body morphogenesis

In addition to notochord-specific Cre expression, we found that some of the transgenic mice expressed Cre in the tail bud from E9.5. This expression pattern correlates with the presence of defective tail somites after E10.5 in some mutants. Hemi-vertebrae in the tail and abnormal vertebrae and scoliosis in the upper spine were observed in the *Itgb1*$^{\Delta ND}$ mutants. The hemi-vertebrae in the tail are possibly

Development (2020) 147, dev192724. doi:10.1242/dev.192724

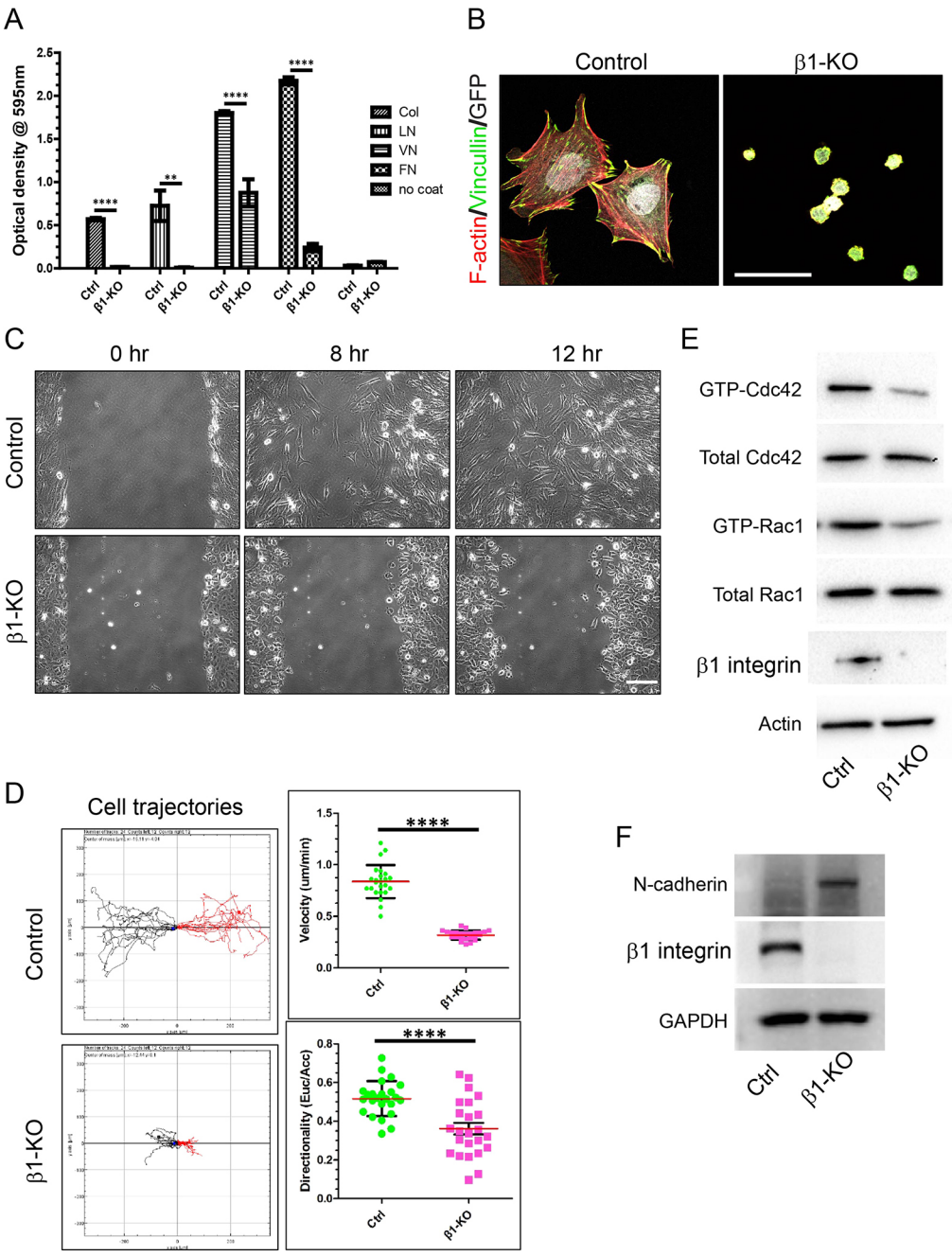

Fig. 8. Decreased cell-matrix interactions in β1-KO cells. (A) Quantification of cell adhesion on indicated substrates for 60 min after seeding. Collagen I (Col), LN, VN and FN. (B) Spreading assay. Cells were stained with vinculin (green) and Phalloidin (red). GFP signal marks the notochordal cell lineages. (C,D) Wound-healing assay: snapshot images of time-lapse movies at the indicated time points are shown (C). Tracking trajectories of the cell moving paths are illustrated in D. (E) Decreased Cdc42 and Rac1 activities in the β1-KO cells when seeding on FN-coated surface. (F) Increased N-cadherin expression in the β1-KO cells. Data are mean±s.d. ***P*<0.005; *****P*<0.0001 (unpaired two-tailed Student's *t*-test). Scale bars: 50 µm for B; 100 µm for C.

due to the combination of Cre activity in the notochord and the tail bud at E9.5, which later affects posterior (tail) somitogenesis. In the mouse, the notochord is the source of SHH signals essential for induction of the floor plate, sclerotome differentiation and subsequent formation of the vertebral column (Echelard et al., 1993; Chamberlain et al., 2008). Removal of *Shh* expression in the notochord resulted in absence of SHH in the floor plate, and loss of the IVDs and vertebral structures, indicating an essential role for a notochordal source of SHH for patterning the spinal column (Choi et al., 2012). It has also been shown that, in the absence of the notochord, the floor plate is sufficient for maintaining differentiation of the somite into the sclerotome and vertebra (Ando et al., 2011). It is interesting that in the *Itgb1*$^{\Delta ND}$ mutants, despite the interruptions in the notochord, induction of the floor plate and neural tube patterning are not perturbed adjacent to regions from which the notochord is absent. This suggests that an initially intact notochord in the *Itgb1*$^{\Delta ND}$ mutants provides sufficient SHH for floor plate induction. This initial source, together with endogenous SHH production within the floor plate, is sufficient to pattern the neural tube.

Although it is not possible to ascribe the tail vertebrae phenotype at birth solely to Cre activity in the notochord, the influence of the notochord on development of the vertebrae cannot be excluded. Lineage tracing for the cells in the node of the late-streak-stage embryo (~E7.5), have been shown to contribute to the anterior notochord. Node cells from more advanced embryos (E7.5-E7.75), including posterior pit and crown cells, also contribute to the notochord in the upper trunk (Tam et al., 1997; Kinder et al., 2001; Robb and Tam, 2004; Yamanaka et al., 2007). Whether descendants of tail bud cells can contribute to thoracic vertebrae is an open question, especially because fate mapping studies using E9.5-E13.5 tail bud cells show contribution to more posterior somites

Development (2020) 147, dev192724. doi:10.1242/dev.192724

(Tam and Tan, 1992). Grafting studies have shown that tail bud cells do not incorporate well to the axis, and tend to contribute to short stretches of somites (Cambray and Wilson, 2002). Therefore, as abnormal vertebrae were also observed in thoracic regions postnatally (Fig. 2B), and displaced notochord segments at the level of future trunk vertebrae were found at E12.5 (Fig. S5), a possible influence of the notochord cannot be excluded.

For the tail, Cre activity in the tail bud may impact the differentiation of posterior somites. This impact, together with interrupted SHH production from the fragmented notochord, is not compensated by the floor plate resulting in abnormal development of the tail IVDs and associated vertebrae, culminating in the morphological abnormalities seen, such as malformed vertebrae and hemi-vertebrae. Combined with the thoracic vertebral defect, our data suggest that the notochord midline position is crucial for the site of IVD formation and the alignment of the vertebral column. Such a scenario provides insight into the anomalies present in the upper spine of *Itgb1*$^{\Delta ND}$ mutants at birth.

Relevance to human congenital spine disorders

The phenotypic consequences of the disrupted notochord and tail defects found in the *Itgb1*$^{\Delta ND}$ mutants suggest a novel mechanism for the pathogenesis of the human congenital disorders, hemi-vertebra and scoliosis. The current study implicates β1 integrin-mediated cell-ECM interactions serving as the safe guardian for the notochord along its journey to NP by maintaining its proper convergent extension, structural integrity and fine-tuned midline position that is essential for the proper formation of the NP in the IVDs. Whether developmental defects in the notochord underlie human congenital spine disorders warrants further investigation. In the future, it would be important to clarify a direct correlation between the embryonic midline position of the notochord with effects on sclerotome differentiation and vertebral body patterning at different levels of the spine, and the relationship to scoliosis.

MATERIALS AND METHODS

Mouse lines

The *Foxa2mNE-Cre* transgenic mice were generated by pronuclear injection into F1 C57/Bl6 X CBA zygotes and maintained in the same F1 background (Au et al., 2020). The floxed β1 integrin line (*β1*$^{F/F}$) and the *zEG* reporter strain have been described previously (Novak et al., 2000; Potocnik et al., 2000). All animals were maintained in the Laboratory of Animal Unit at the University of Hong Kong. Animal care and experiments performed were in accordance with the protocols approved by the Committee on the Use of Live Animals in Teaching and Research of the University of Hong Kong.

Skeletal preparations and analyses

P20 control and *Itgb1*$^{\Delta ND}$ mutant mice were eviscerated, fixed in 100% ethanol and transferred to acetone solution. Specimens were rinsed with water and stained in Alcian Blue/Alizarin Red solution (McLeod, 1980) for 10 days before clearing and storing in 100% glycerol for photography.

Mosaicism measurement

The frequency of mosaicism was defined by the ratio between the cell numbers with mosaic β1 integrin expression and the total cell numbers that were DAPI+T+. Signal intensities were measured using ImageJ. Cells with an intensity <20 arbitrary units (a.u.) were grouped into 'complete knockout', >20 a.u. were grouped into 'mosaic expression' (Fig. S2A).

WISH

WISH was carried out with modifications on the standard protocol (Wilkinson, 1992) using digoxigenin (DIG)-labeled riboprobes specific for transcripts of *T* (Wilkinson et al., 1990), *Noto* (Abdelkhalek et al., 2004), *Shh* (Echelard et al., 1993), *Uncx4.1* (Mansouri et al., 1997) and *Pax1* (Deutsch et al., 1988). Anti–DIG-AP antibody (#11093274910, Roche, 1:2000) and BM Purple (#11442074001, Roche, ready-to-use solution) were used for signal detection.

BrdU and EdU incorporation assay

Cell proliferation activity was analyzed using BrdU or EdU labeling assays. Mice were injected intraperitoneally with 200 µg of BrdU or EdU per gram of body weight 2 h before sacrifice. Following fixation, BrdU incorporation in paraffin sections from E9.5 embryos was detected using a BrdU Staining Kit (93-3943, Thermo Fisher Scientific). EdU incorporation on E8.5 embryos was detected using Click-iT™ EdU Alexa Fluor™ 488 Imaging Kit (C10337, Thermo Fisher Scientific).

Immunostaining and confocal microscopy

Tissue sections, cells or embryos underwent immunostaining with the following antibodies: integrin β1 (Millipore, MAB1997, 1:400), brachyury (Santa Cruz Biotechnology, SC-17745, 1:200), Foxa2 (Santa Cruz Biotechnology, SC-101060, 1:200), laminin (Sigma-Aldrich, L9393, 1:800), fibronectin (Millipore, Ab2033, 1:400), vincullin (Sigma-Aldrich, V9131, 1:500), Phalloidin Alexa 546 (Thermo Fisher Scientific, A22283, 1:500), N-cadherin (BD Transduction Laboratories, 610920, 1:800), SOX9 (Millipore, Ab5535, 1:1000), GFP (Abcam, ab6556, 1:1000), active caspase 3 (Cell Signaling Technologies, #9661, 1:100). VANGL2 antibody (rabbit, 1:800) was a kind gift from Dr Matthew W. Kelley (National Institutes of Health, Bethesda, MD, USA).

For whole-mount embryo staining, the embryos were dissected out followed by the removal of the head and the heart for the flat mount at the end. Embryos were permeabilized with 0.5% Triton X-100 (v/v) in PBS for 30 min before antibody application. Both primary and secondary antibodies were incubated overnight at 4°C.

Fluorescent images were obtained using a Carl Zeiss LSM700 or LSM780 microscope maintained by the University of Hong Kong Li Ka Shing Faculty of Medicine Faculty Core Facility.

Time-lapse live imaging of the mouse embryos

Imaging was set up following protocols described previously (Yamanaka et al., 2007; Imuta et al., 2014). Embryos at stages between ∼E7.75-E8.0 (∼1 s) were dissected in F12 with 10% fetal bovine serum (FBS) and 15 mM HEPES and were held within the home-made sticky edges on the CoverWell perfusion chamber gaskets (Fig. S9A). Embryos were then cultured in 50% rat serum (v/v), 50% dissection medium (v/v) without Phenol Red supplemented with 100 µM of 2-mercaptoethanol and 1 mM of sodium pyruvate in 5% CO_2 in air at 37°C. A thin layer of miner oil was applied to the medium surface to avoid evaporation.

Embryos were allowed to recover for ∼1 h in the rotating culture system before imaging. Time-lapse live images were acquired using an inverted microscope (LSM510, Carl Zeiss) equipped with an incubator unit, a 488-nm diode laser and a 20× lens (NA=0.75). The cells within both the notochord and the node were imaged for 16.8 h. Images were acquired every 10 min, with ∼16-23 *z*-positions at each time point, and the section interval was 10 µm. Drift in embryo positioning during imaging was corrected manually based on the non-moving or slow-moving cells and the midline axis at every consecutive time point. Cell moving behaviors were tracked and analyzed via ImageJ. The parameters analyzed are illustrated in Fig. S9B.

Rotating embryo culture

Wild-type embryos at stages ∼E7.25 were dissected in the medium mentioned above. Then 20 µg/ml functional blocking antibodies (BD Pharmingen, 555002, 1:50) or the corresponding IgM isotype control (BD Pharmingen, 553957, 1:50) were applied to the embryos and cultured with a rotating system with 5% CO_2 in air at 37°C with the medium described above. Embryos were harvested 24 h later, stained and flat-mounted for confocal imaging.

Notochordal cell isolation, immortalization and Crispr-Cas9 knockout

Notochordal cells were GFP-labeled by intercrossing the *Foxa2mNE-Cre* line with an EGFP Cre reporter strain (*zEG*) (Novak et al., 2000). Notochord-containing tissues were collected from ∼20 embryos at E9.5 and

Development (2020) 147, dev192724. doi:10.1242/dev.192724

trypsin digested for 15 min at room temperature. Notochordal cells were then enriched by GFP cell sorting and immortalized by retrovirally transducing the SV40 large T antigen.

Two guide RNA sequences (gRNAs) targeting mouse *Itgb1* were synthesized and cloned into pSpCas9(BB)-2A-Puro (PX459) V2.0 (Ran et al., 2013). gRNA-1: CAAACTGATCAATCCAATCC; gRNA-2: TATACATTCTCCGCAAGATT. Puromycin at 3 µg/ml was used to screen the positive clones. Knockout clones from both gRNAs displayed similar morphologies and defects in cell spreading. Data presented here show the knockout clone from gRNA-1.

Flow cytometry

For integrin expression profiling, after trypsinization and washing, notochordal cells were stained with PE-conjugated or non-conjugated integrin antibodies diluted (1:200) in FACS buffer [1% bovine serum albumin (BSA) in PBS] for 30 min in dark on ice, washed twice with ice-cold FACS buffer. The secondary antibody was incubated for another 30 min if necessary. Flow cytometry was analyzed using a flow cytometer (FACSCanto II; BD Biosciences).

FACS antibodies used: anti-β1 integrin (HMβ1-1, BioLegend, 102207), anti-β2 integrin (C71/16, BD Biosciences, 553293), anti-β3 integrin (2C9.G3, eBioscience, 12-0611), anti-β4 integrin (346-11A, Serotec, MCA2369PE), anti-β7 integrin (M293, BD Biosciences, 557498), anti-α1 integrin (Ha31/8, BD Biosciences, 555001), anti-α4 integrin (R1-2, BD Biosciences, 553157), anti-α5 integrin (5H10-27, BD Biosciences, 557447), anti-αV integrin (RMV-7; BD Biosciences, 551187) and anti-α6 integrin (GoH3, BD Biosciences, 555736). Isotype control antibodies: rat IgG2b (eB149/10H5, eBioscience, 12-4031), rat IgG1 (R3-34, BD Biosciences, 554685), rat IgG2a, K (R35-95, BD Biosciences, 555844), rat IgG2a (YTH71.3, Serotec, MCA1212PE) and hamster IgG (eBio299Arm, eBioscience, 12-4888-83).

Adhesion, spreading and scratch-induced migration assay

All substrates were coated at a concentration of 5 µg/ml overnight at 4°C. The coating substrates used in this assay were fibronectin (Sigma-Aldrich, F1141), vitronectin (Stem Cell Technologies, 07180), laminin (Life Technologies, 23017-15) and collagen (Advanced Biomatrix, 5005-100 ml). A 96-well plate was blocked with 1% BSA in PBS for ∼2 h before cell seeding. Cells were seeded at a density of 50,000 cell/well in DMEM with 1% FBS and placed in the incubator for 60 min for adhesion. Unbound cells were washed away, and the bound cells were fixed and stained at 4°C overnight with 0.1% Cristal-Violet (w/v) in 20% methanol (v/v). Cells were then permeabilized with 0.1% Triton X-100 (v/v) for 5 h at room temperature and the optical density was recorded under 595 nm.

Control or β1-KO cells were allowed to spread on the FN-coated surface (5 µg/ml) for 90 min before the analysis of the focal adhesion formation and the cytoskeleton organization. Cells were allowed to grow into ∼90% confluency in the six-well plastic well before scratching. For each well, two scratches were made using 200 µl pipette tips. Detached cells were washed away with warm PBS, and the wound closure was started in DMEM with 1% FBS. Then the cells were time-lapse live imaged under the wide-field lens using a Perkin-Elmer ultraView ERS spinning disk system attached to a ZEISS Axio Observer microscope with an EM CCD camera. Imaging was acquired with a Plan Neofluar 10×0.3 NA objective in 12 different microscopic fields at a 10 min interval overnight. Cell moving behaviors were tracked and analyzed using ImageJ.

Assays on the small GTPase activities

To analyze the activities of Rac1 and Cdc42, control and β1-KO notochord cells were grown to ∼80% confluency and serum starved in DMEM with 0.5% BSA for 24 h. Cells were then trypsinized and suspended for 3 h in serum-free DMEM containing 0.1% BSA and 0.25 mg/ml soybean trypsin inhibitor (Life Technologies, 17075-029). Cells were then plated to dishes that had been coated with 20 µg/ml FN and blocked with 1% BSA. Cells were allowed to adhere to FN for 10 min, then were washed with 10 ml ice-cold PBS and extracted in lysis buffer [25 mM Tris HCl, 150 mM NaCl, 5 mM $MgCl_2$, 1% NP40 (v/v), 5% glycerol (v/v) (pH 7.2)] with proteinase inhibitors (Roche, 11873580001) and phosphatase inhibitors (sodium orthovanadate at 1 mM, Sigma-Aldrich, S6508). Rac1 and Cdc42 activities were tested via the detection kits from Cell Signaling Technologies (#8815 and #8819) and analyzed via western blot.

Antibodies used for western blot were: integrin β1 (Millipore, MAB1997, 1:2000), N-cadherin (BD Transduction Laboratories, 610920, 1:2000), actin (Sigma-Aldrich, A2228, 1:5000) and GAPDH (Calbiochem, CB1001, 1:10,000).

Statistical analysis

Statistical analysis was performed using GraphPad Prism 6. For every reported dataset at least three independent experiments were performed, except for Fig. S11. Statistical significance was assumed at $P<0.05$. *$P<0.05$; **$P<0.005$; ***$P<0.0005$ and ****$P<0.0001$. Statistical tests used for the experiments are described in the figure legends. Unless otherwise noted, all values are reported as mean±s.d.

Acknowledgements

We are grateful to Matthew W. Kelly for the gift of VANGL2 antibodies, Xiaochen Lin for the N-cadherin expression analysis *in vitro*, Ralph Thomas Böttcher for flow cytometry analysis, Zhiqi Sun for advice and for critical reading of the manuscript, Bo Gao and Patrick Tam for helpful and critical discussion.

Competing interests

The authors declare no competing or financial interests.

Author contributions

Conceptualization: S.S.G., R.F., K.S.E.C.; Methodology: S.S.G., T.Y.K.A., S.W., A.A., K.S.E.C.; Investigation: S.S.G., T.Y.K.A., S.W., A.A.; Data curation: S.S.G., A.A., D.C., R.F., K.S.E.C.; Writing - original draft: S.S.G., K.S.E.C.; Writing - review & editing: S.S.G., A.A., D.C., R.F., K.S.E.C.; Supervision: R.F., K.S.E.C.; Funding acquisition: K.S.E.C.

Funding

This study is supported by the University Grants Committee and Research Grants Council, University Grants Committee of Hong Kong (AoE/M-04/04) and Research Grants of Hong Kong (T12-708/12-N).

Supplementary information

Supplementary information available online at
https://dev.biologists.org/lookup/doi/10.1242/dev.192724.supplemental

Peer review history

The peer review history is available online at
https://dev.biologists.org/lookup/doi/10.1242/dev.192724.reviewer-comments.pdf

References

Abdelkhalek, H. B., Beckers, A., Schuster-Gossler, K., Pavlova, M. N., Burkhardt, H., Lickert, H., Rossant, J., Reinhardt, R., Schalkwyk, L. C., Muller, I. et al. (2004). The mouse homeobox gene Not is required for caudal notochord development and affected by the truncate mutation. *Genes Dev.* **18**, 1725-1736. doi:10.1101/gad.303504

Ando, T., Semba, K., Suda, H., Sei, A., Mizuta, H., Araki, M., Abe, K., Imai, K., Nakagata, N., Araki, K. et al. (2011). The floor plate is sufficient for development of the sclerotome and spine without the notochord. *Mech. Dev.* **128**, 129-140. doi:10.1016/j.mod.2010.11.005

Aszódi, A., Chan, D., Hunziker, E., Bateman, J. F. and Fässler, R. (1998). Collagen II is essential for the removal of the notochord and the formation of intervertebral discs. *J. Cell Biol.* **143**, 1399-1412. doi:10.1083/jcb.143.5.1399

Au, T., Lam, T. K., Peng, Y., Wynn, S., Cheung, K., Cheah, K. S. E. and Leung, V. (2020). Transformation of resident notochord-descendent nucleus pulposus cells in mouse injury-induced fibrotic intervertebral discs. *Aging Cell*, e13254. doi:10.1111/acel.13254

Balmer, S., Nowotschin, S. and Hadjantonakis, A.-K. (2016). Notochord morphogenesis in mice: Current understanding & open questions. *Dev. Dyn.* **245**, 547-557. doi:10.1002/dvdy.24392

Bellomo, D., Lander, A., Harragan, I. and Brown, N. A. (1996). Cell proliferation in mammalian gastrulation: the ventral node and notochord are relatively quiescent. *Dev. Dyn.* **205**, 471-485. doi:10.1002/(SICI)1097-0177(199604)205:4<471::AID-AJA10>3.0.CO;2-4

Brakebusch, C., Grose, R., Quondamatteo, F., Ramirez, A., Jorcano, J. L., Pirro, A., Svensson, M., Herken, R., Sasaki, T., Timpl, R. et al. (2000). Skin and hair follicle integrity is crucially dependent on β1 integrin expression on keratinocytes. *EMBO J.* **19**, 3990-4003. doi:10.1093/emboj/19.15.3990

Briscoe, J., Sussel, L., Serup, P., Hartigan-O'Connor, D., Jessell, T. M., Rubenstein, J. L. and Ericson, J. (1999). Homeobox gene Nkx2.2 and

specification of neuronal identity by graded Sonic hedgehog signalling. *Nature* **398**, 622-627. doi:10.1038/19315

Briscoe, J., Pierani, A., Jessell, T. M. and Ericson, J. (2000). A homeodomain protein code specifies progenitor cell identity and neuronal fate in the ventral neural tube. *Cell* **101**, 435-445. doi:10.1016/S0092-8674(00)80853-3

Cambray, N. and Wilson, V. (2002). Axial progenitors with extensive potency are localised to the mouse chordoneural hinge. *Development* **129**, 4855-4866.

Chamberlain, C. E., Jeong, J., Guo, C., Allen, B. L. and McMahon, A. P. (2008). Notochord-derived Shh concentrates in close association with the apically positioned basal body in neural target cells and forms a dynamic gradient during neural patterning. *Development* **135**, 1097-1106. doi:10.1242/dev.013086

Choi, K.-S., Cohn, M. J. and Harfe, B. D. (2008). Identification of nucleus pulposus precursor cells and notochordal remnants in the mouse: implications for disk degeneration and chordoma formation. *Dev. Dyn.* **237**, 3953-3958. doi:10.1002/dvdy.21805

Choi, K.-S., Lee, C. and Harfe, B. D. (2012). Sonic hedgehog in the notochord is sufficient for patterning of the intervertebral discs. *Mech. Dev.* **129**, 255-262. doi:10.1016/j.mod.2012.07.003

Corallo, D., Trapani, V. and Bonaldo, P. (2015). The notochord: structure and functions. *Cell. Mol. Life Sci.* **72**, 2989-3008. doi:10.1007/s00018-015-1897-z

Deutsch, U., Dressler, G. R. and Gruss, P. (1988). Pax 1, a member of a paired box homologous murine gene family, is expressed in segmented structures during development. *Cell* **53**, 617-625. doi:10.1016/0092-8674(88)90577-6

Dray, N., Lawton, A., Nandi, A., Jülich, D., Emonet, T. and Holley, S. A. (2013). Cell-fibronectin interactions propel vertebrate trunk elongation via tissue mechanics. *Curr. Biol.* **23**, 1335-1341. doi:10.1016/j.cub.2013.05.052

Dzamba, B. J., Jakab, K. R., Marsden, M., Schwartz, M. A. and DeSimone, D. W. (2009). Cadherin adhesion, tissue tension, and noncanonical Wnt signaling regulate fibronectin matrix organization. *Dev. Cell* **16**, 421-432. doi:10.1016/j.devcel.2009.01.008

Echelard, Y., Epstein, D. J., St-Jacques, B., Shen, L., Mohler, J., McMahon, J. A. and McMahon, A. P. (1993). Sonic hedgehog, a member of a family of putative signaling molecules, is implicated in the regulation of CNS polarity. *Cell* **75**, 1417-1430. doi:10.1016/0092-8674(93)90627-3

Ericson, J., Briscoe, J., Rashbass, P., van Heyningen, V. and Jessell, T. M. (1997). Graded sonic hedgehog signaling and the specification of cell fate in the ventral neural tube. *Cold Spring Harb. Symp. Quant. Biol.* **62**, 451-466. doi:10.1101/SQB.1997.062.01.053

Ezin, A. M., Skoglund, P. and Keller, R. (2003). The midline (notochord and notoplate) patterns the cell motility underlying convergence and extension of the Xenopus neural plate. *Dev. Biol.* **256**, 100-114. doi:10.1016/S0012-1606(02)00130-6

Fassler, R. and Meyer, M. (1995). Consequences of lack of beta 1 integrin gene expression in mice. *Genes Dev.* **9**, 1896-1908. doi:10.1101/gad.9.15.1896

Frisch, S. M. and Ruoslahti, E. (1997). Integrins and anoikis. *Curr. Opin. Cell Biol.* **9**, 701-706. doi:10.1016/S0955-0674(97)80124-X

George, E. L., Georges-Labouesse, E. N., Patel-King, R. S., Rayburn, H. and Hynes, R. O. (1993). Defects in mesoderm, neural tube and vascular development in mouse embryos lacking fibronectin. *Development* **119**, 1079-1091.

Goto, T., Davidson, L., Asashima, M. and Keller, R. (2005). Planar cell polarity genes regulate polarized extracellular matrix deposition during frog gastrulation. *Curr. Biol.* **15**, 787-793. doi:10.1016/j.cub.2005.03.040

Gotz, W., Osmers, R. and Herken, R. (1995). Localisation of extracellular matrix components in the embryonic human notochord and axial mesenchyme. *J. Anat.* **186**, 111-121.

Gray, R. S., Roszko, I. and Solnica-Krezel, L. (2011). Planar cell polarity: coordinating morphogenetic cell behaviors with embryonic polarity. *Dev. Cell* **21**, 120-133. doi:10.1016/j.devcel.2011.06.011

Hashimoto, M., Shinohara, K., Wang, J., Ikeuchi, S., Yoshiba, S., Meno, C., Nonaka, S., Takada, S., Hatta, K., Wynshaw-Boris, A. et al. (2010). Planar polarization of node cells determines the rotational axis of node cilia. *Nat. Cell Biol.* **12**, 170-176. doi:10.1038/ncb2020

Heisenberg, C.-P., Tada, M., Rauch, G.-J., Saúde, L., Concha, M. L., Geisler, R., Stemple, D. L., Smith, J. C. and Wilson, S. W. (2000). Silberblick/Wnt11 mediates convergent extension movements during zebrafish gastrulation. *Nature* **405**, 76-81. doi:10.1038/35011068

Hynes, R. O. (2002). Integrins: bidirectional, allosteric signaling machines. *Cell* **110**, 673-687. doi:10.1016/S0092-8674(02)00971-6

Imuta, Y., Koyama, H., Shi, D., Eiraku, M., Fujimori, T. and Sasaki, H. (2014). Mechanical control of notochord morphogenesis by extra-embryonic tissues in mouse embryos. *Mech. Dev.* **132**, 44-58. doi:10.1016/j.mod.2014.01.004

Jessell, T. M., Bovolenta, P., Placzek, M., Tessier-Lavigne, M. and Dodd, J. (1989). Polarity and patterning in the neural tube: the origin and function of the floor plate. *Ciba Found. Symp.* **144**, 255-276; discussion 276-280, 290-255.

Jurand, A. (1974). Some aspects of the development of the notochord in mouse embryos. *J. Embryol. Exp. Morphol.* **32**, 1-33.

Kilian, B., Mansukoski, H., Barbosa, F. C., Ulrich, F., Tada, M. and Heisenberg, C.-P. (2003). The role of Ppt/Wnt5 in regulating cell shape and movement during zebrafish gastrulation. *Mech. Dev.* **120**, 467-476. doi:10.1016/S0925-4773(03)00004-2

Kim, J., Mohanty, S., Ganesan, L. P., Hua, K., Jarjoura, D., Hayton, W. L., Robinson, J. M. and Anderson, C. L. (2009). FcRn in the yolk sac endoderm of mouse is required for IgG transport to fetus. *J. Immunol.* **182**, 2583-2589. doi:10.4049/jimmunol.0803247

Kinder, S. J., Tsang, T. E., Wakamiya, M., Sasaki, H., Behringer, R. R., Nagy, A. and Tam, P. P. (2001). The organizer of the mouse gastrula is composed of a dynamic population of progenitor cells for the axial mesoderm. *Development* **128**, 3623-3634.

Lawson, L. and Harfe, B. D. (2015). Notochord to nucleus pulposus transition. *Curr. Osteoporos Rep.* **13**, 336-341. doi:10.1007/s11914-015-0284-x

Legate, K. R., Montañez, E., Kudlacek, O. and Füssler, R. (2006). ILK, PINCH and parvin: the tIPP of integrin signalling. *Nat. Rev. Mol. Cell Biol.* **7**, 20-31. doi:10.1038/nrm1789

Mahaffey, J. P., Grego-Bessa, J., Liem, K. F., Jr and Anderson, K. V. (2013). Cofilin and Vangl2 cooperate in the initiation of planar cell polarity in the mouse embryo. *Development* **140**, 1262-1271. doi:10.1242/dev.085316

Mansouri, A., Yokota, Y., Wehr, R., Copeland, N. G., Jenkins, N. A. and Gruss, P. (1997). Paired-related murine homeobox gene expressed in the developing sclerotome, kidney, and nervous system. *Dev. Dyn.* **210**, 53-65. doi:10.1002/(SICI)1097-0177(199709)210:1<53::AID-AJA6>3.0.CO;2-0

Marsden, M. and DeSimone, D. W. (2003). Integrin-ECM interactions regulate cadherin-dependent cell adhesion and are required for convergent extension in Xenopus. *Curr. Biol.* **13**, 1182-1191. doi:10.1016/S0960-9822(03)00433-0

Merad, Z. and Wild, A. E. (1992). The route of maternal IgM transport to the rabbit fetus. *Placenta* **13**, 291-304. doi:10.1016/0143-4004(92)90044-T

McCann, M. R., Tamplin, O. J., Rossant, J. and Seguin, C. A. (2012). Tracing notochord-derived cells using a Noto-cre mouse: implications for intervertebral disc development. *Dis. Model. Mech.* **5**, 73-82. doi:10.1242/dmm.008128

McLeod, M. J. (1980). Differential staining of cartilage and bone in whole mouse fetuses by alcian blue and alizarin red S. *Teratology* **22**, 299-301. doi:10.1002/tera.1420220306

Novak, A., Guo, C., Yang, W., Nagy, A. and Lobe, C. G. (2000). Z/EG, a double reporter mouse line that expresses enhanced green fluorescent protein upon Cre-mediated excision. *Genesis* **28**, 147-155. doi:10.1002/1526-968X(200011/12)28:3/4<147::AID-GENE90>3.0.CO;2-G

Park, M. and Moon, R. T. (2002). The planar cell-polarity gene stbm regulates cell behaviour and cell fate in vertebrate embryos. *Nat. Cell Biol.* **4**, 20-25. doi:10.1038/ncb716

Parsons, M. J., Pollard, S. M., Saude, L., Feldman, B., Coutinho, P., Hirst, E. M. and Stemple, D. L. (2002). Zebrafish mutants identify an essential role for laminins in notochord formation. *Development* **129**, 3137-3146.

Potocnik, A. J., Brakebusch, C. and Fässler, R. (2000). Fetal and adult hematopoietic stem cells require beta1 integrin function for colonizing fetal liver, spleen, and bone marrow. *Immunity* **12**, 653-663. doi:10.1016/S1074-7613(00)80216-2

Pourquie, O., Coltey, M., Teillet, M. A., Ordahl, C. and Le Douarin, N. M. (1993). Control of dorsoventral patterning of somitic derivatives by notochord and floor plate. *Proc. Natl. Acad. Sci. USA* **90**, 5242-5246. doi:10.1073/pnas.90.11.5242

Pulina, M., Liang, D. and Astrof, S. (2014). Shape and position of the node and notochord along the bilateral plane of symmetry are regulated by cell-extracellular matrix interactions. *Biol. Open* **3**, 583-590. doi:10.1242/bio.20148243

Ran, F. A., Hsu, P. D., Wright, J., Agarwala, V., Scott, D. A. and Zhang, F. (2013). Genome engineering using the CRISPR-Cas9 system. *Nat. Protoc.* **8**, 2281-2308. doi:10.1038/nprot.2013.143

Robb, L. and Tam, P. P. (2004). Gastrula organiser and embryonic patterning in the mouse. *Semin. Cell Dev. Biol.* **15**, 543-554. doi:10.1016/j.semcdb.2004.04.005

Roberts, D. M., Guenthert, M. and Rodewald, R. (1990). Isolation and characterization of the Fc receptor from the fetal yolk sac of the rat. *J. Cell Biol.* **111**, 1867-1876. doi:10.1083/jcb.111.5.1867

Roelink, H., Porter, J. A., Chiang, C., Tanabe, Y., Chang, D. T., Beachy, P. A. and Jessell, T. M. (1995). Floor plate and motor neuron induction by different concentrations of the amino-terminal cleavage product of sonic hedgehog autoproteolysis. *Cell* **81**, 445-455. doi:10.1016/0092-8674(95)90397-6

Rossant, J. and Tam, P. P. L. (2002). *Mouse Development: Patterning, Morphogenesis, and Organogenesis*: Gulf Professional Publishing.

Sasaki, H. and Hogan, B. L. (1996). Enhancer analysis of the mouse HNF-3 beta gene: regulatory elements for node/notochord and floor plate are independent and consist of multiple sub-elements. *Genes Cells* **1**, 59-72. doi:10.1046/j.1365-2443.1996.04004.x

Sausedo, R. A. and Schoenwolf, G. C. (1994). Quantitative analyses of cell behaviors underlying notochord formation and extension in mouse embryos. *Anat. Rec.* **239**, 103-112. doi:10.1002/ar.1092390112

Segade, F., Cota, C., Famiglietti, A., Cha, A. and Davidson, B. (2016). Fibronectin contributes to notochord intercalation in the invertebrate chordate, Ciona intestinalis. *Evodevo* **7**, 21. doi:10.1186/s13227-016-0056-4

Smits, P. and Lefebvre, V. (2003). Sox5 and Sox6 are required for notochord extracellular matrix sheath formation, notochord cell survival and development of

the nucleus pulposus of intervertebral discs. *Development* **130**, 1135-1148. doi:10.1242/dev.00331

Song, H., Hu, J., Chen, W., Elliott, G., Andre, P., Gao, B. and Yang, Y. (2010). Planar cell polarity breaks bilateral symmetry by controlling ciliary positioning. *Nature* **466**, 378-382. doi:10.1038/nature09129

Stemple, D. L. (2005). Structure and function of the notochord: an essential organ for chordate development. *Development* **132**, 2503-2512. doi:10.1242/dev.01812

Stephens, L. E., Sutherland, A. E., Klimanskaya, I. V., Andrieux, A., Meneses, J., Pedersen, R. A. and Damsky, C. H. (1995). Deletion of beta 1 integrins in mice results in inner cell mass failure and peri-implantation lethality. *Genes Dev.* **9**, 1883-1895. doi:10.1101/gad.9.15.1883

Sulik, K., Dehart, D. B., Iangaki, T., Carson, J. L., Vrablic, T., Gesteland, K. and Schoenwolf, G. C. (1994). Morphogenesis of the murine node and notochordal plate. *Dev. Dyn.* **201**, 260-278. doi:10.1002/aja.1002010309

Sun, Z., Guo, S. S. and Fässler, R. (2016). Integrin-mediated mechanotransduction. *J. Cell Biol.* **215**, 445-456. doi:10.1083/jcb.201609037

Sutherland, A., Keller, R. and Lesko, A. (2020). Convergent extension in mammalian morphogenesis. *Semin. Cell Dev. Biol.* **100**, 199-211. doi:10.1016/j.semcdb.2019.11.002

Tada, M. and Heisenberg, C.-P. (2012). Convergent extension: using collective cell migration and cell intercalation to shape embryos. *Development* **139**, 3897-3904. doi:10.1242/dev.073007

Tam, P. P., Steiner, K. A., Zhou, S. X. and Quinlan, G. A. (1997). Lineage and functional analyses of the mouse organizer. *Cold Spring Harb. Symp. Quant. Biol.* **62**, 135-144. doi:10.1101/SQB.1997.062.01.018

Tam, P. P. and Tan, S. S. (1992). The somitogenetic potential of cells in the primitive streak and the tail bud of the organogenesis-stage mouse embryo. *Development* **115**, 703-715.

Trapani, V., Bonaldo, P. and Corallo, D. (2017). Role of the ECM in notochord formation, function and disease. *J. Cell Sci.* **130**, 3203-3211. doi:10.1242/jcs.175950

Torban, E., Patenaude, A.-M., Leclerc, S., Rakowiecki, S., Gauthier, S., Andelfinger, G., Epstein, D. J. and Gros, P. (2008). Genetic interaction between members of the Vangl family causes neural tube defects in mice. *Proc. Natl. Acad. Sci. USA* **105**, 3449-3454. doi:10.1073/pnas.0712126105

Ukita, K., Hirahara, S., Oshima, N., Imuta, Y., Yoshimoto, A., Jang, C.-W., Oginuma, M., Saga, Y., Behringer, R. R., Kondoh, H. et al. (2009). Wnt signaling maintains the notochord fate for progenitor cells and supports the posterior extension of the notochord. *Mech. Dev.* **126**, 791-803. doi:10.1016/j.mod.2009.08.003

Varras, M. and Akrivis, C. (2010). Prenatal diagnosis of fetal hemivertebra at 20 weeks' gestation with literature review. *Intl. J. Gen. Med.* **3**, 197-201. doi:10.2147/IJGM.S11532

Wilkinson, D. G. (1992). Whole Mount in situ hybridization of vertebrate embryos. In *In Situ Hybridization: A Practical Approach* (ed. D. G. Wilkinson), pp. 75-83. Oxford: IRL Press.

Wilkinson, D. G., Bhatt, S. and Herrmann, B. G. (1990). Expression pattern of the mouse T gene and its role in mesoderm formation. *Nature* **343**, 657-659. doi:10.1038/343657a0

Yamada, T., Placzek, M., Tanaka, H., Dodd, J. and Jessell, T. M. (1991). Control of cell pattern in the developing nervous system: polarizing activity of the floor plate and notochord. *Cell* **64**, 635-647. doi:10.1016/0092-8674(91)90247-V

Yamanaka, Y., Tamplin, O. J., Beckers, A., Gossler, A. and Rossant, J. (2007). Live imaging and genetic analysis of mouse notochord formation reveals regional morphogenetic mechanisms. *Dev. Cell* **13**, 884-896. doi:10.1016/j.devcel.2007.10.016

Yang, Y. and Mlodzik, M. (2015). Wnt-Frizzled/planar cell polarity signaling: cellular orientation by facing the wind (Wnt). *Annu. Rev. Cell Dev. Biol.* **31**, 623-646. doi:10.1146/annurev-cellbio-100814-125315

Yen, W. W., Williams, M., Periasamy, A., Conaway, M., Burdsal, C., Keller, R., Lu, X. and Sutherland, A. (2009). PTK7 is essential for polarized cell motility and convergent extension during mouse gastrulation. *Development* **136**, 2039-2048. doi:10.1242/dev.030601

Figure S1

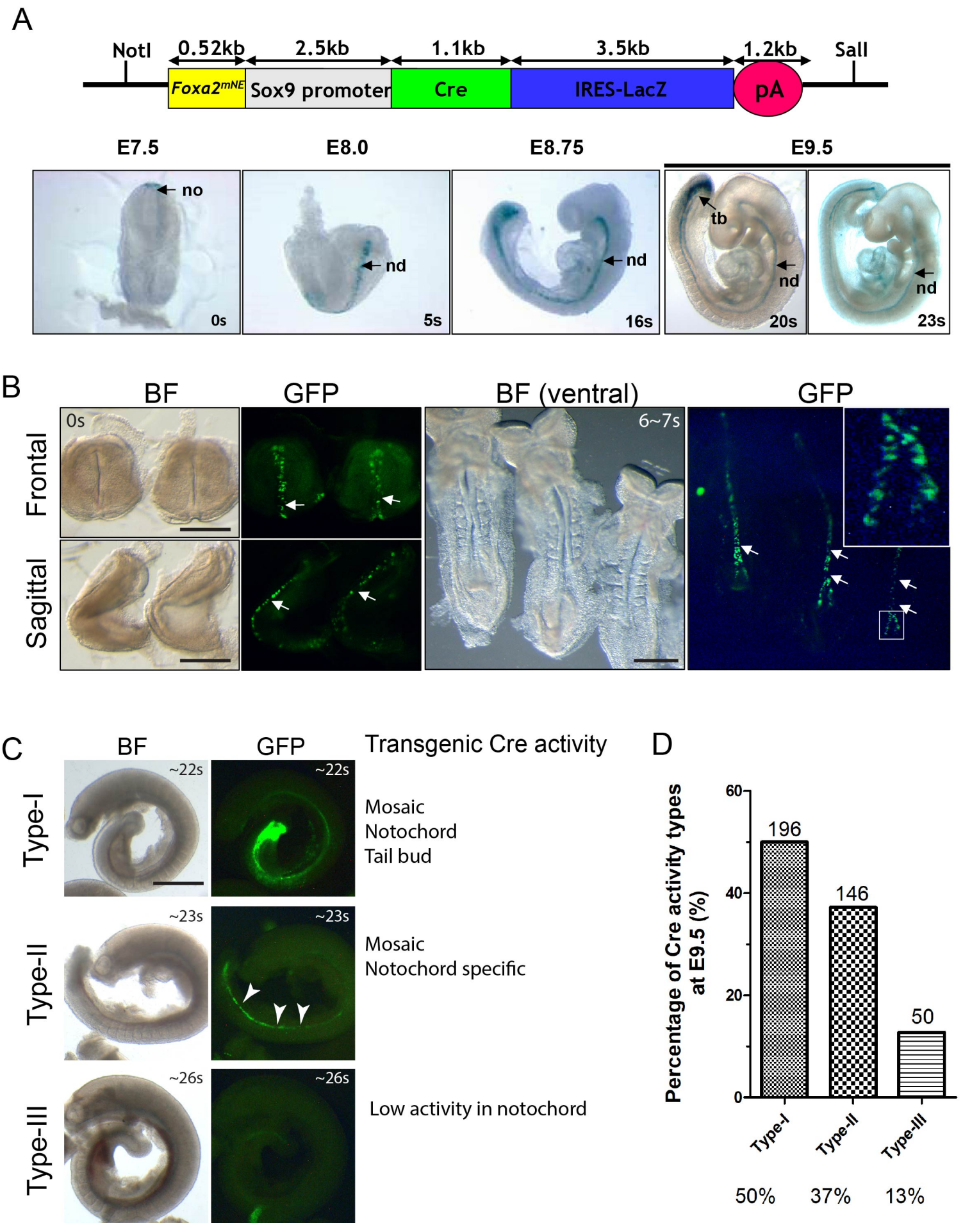

Figure S1: Transgenic notochord-specific Cre expression and activities. (A) Schematic representation of the *Foxa2mNE-Cre* construct. The Cre expression is driven by the *Sox9* promoter together with a notochord enhancer element. An IRES-*lacZ* gene was fused to mark the Cre expression. Shown here is the Cre expression from E7.5 to E9.5. Note that two expression patterns were observed at E9.5. One type with Cre expression in both tail bud (tb) and the notochord (nd), and another type with Cre expression restricted in notochord. (B) Closer look at the Cre activities marked by GFP signals at E8.0 and at E8.5. White arrows indicate the regions without Cre activities. No Cre activity in the pit cells within the center of the node (highlighted in white rectangle). Embryo stages are indicated with somite numbers. Bright field (BF) and GFP field images are shown. (C) Types of Cre activities observed at E9.5. BF and GFP field images are shown for each representative type. Cre activities for each type are described on the right hand side. Arrowheads: regions with no Cre activities. (D) Ratio of each type of Cre activities was quantified based on the observation on 392 embryos from different male breeders. The total count for each type is labelled on top and the ratio was plotted for each type. Scale bars: 1 mm.

Figure S2

A

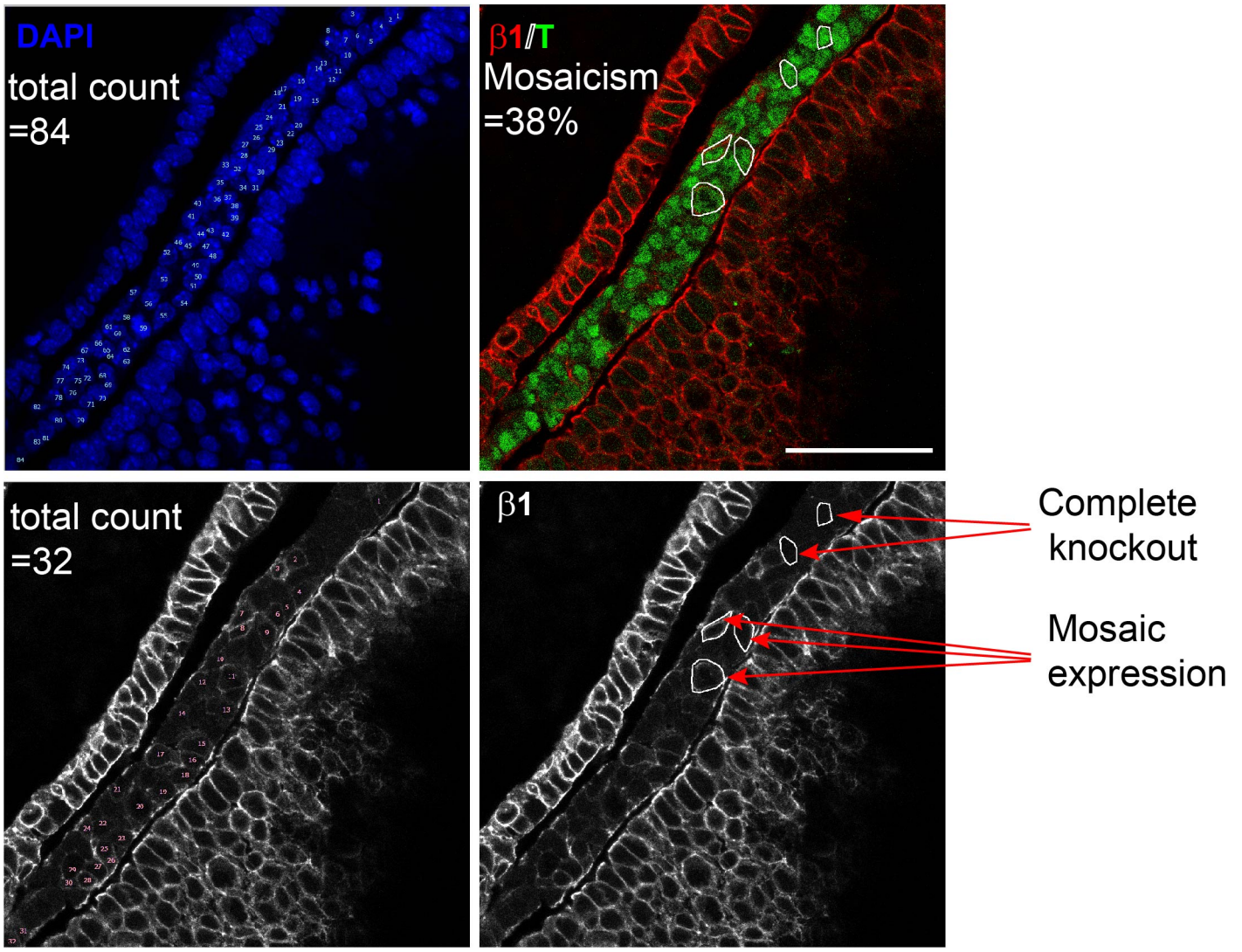

B

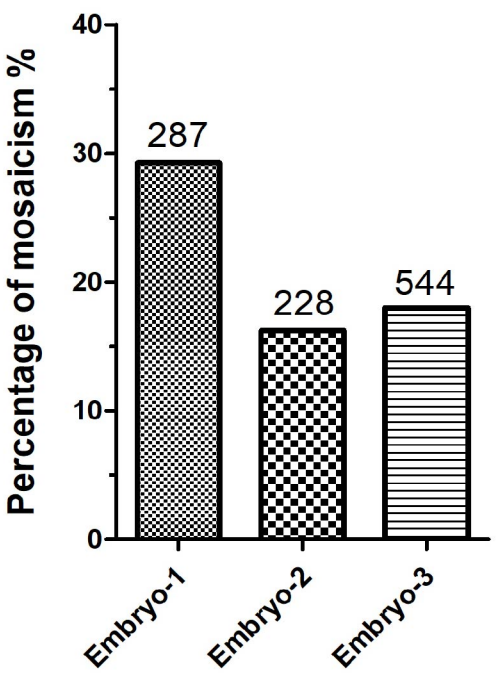

Figure S2: Variable mosaicism observed at E9.5 embryos. (A) Example images showing the calculation of the mosaicism in each image or each embryo. Cell numbers with mosaic β1 integrin expression were divided by the cell numbers that were DAPI/T +. Signal intensities were measured by ImageJ. Cells with an intensity <20 a.u. were grouped into "complete knockout", >20 a.u. were grouped into "mosaic expression". (B) Mosaicism counted for 3 different embryos at E9.5. Scale bar: 50 μm.

Figure S3

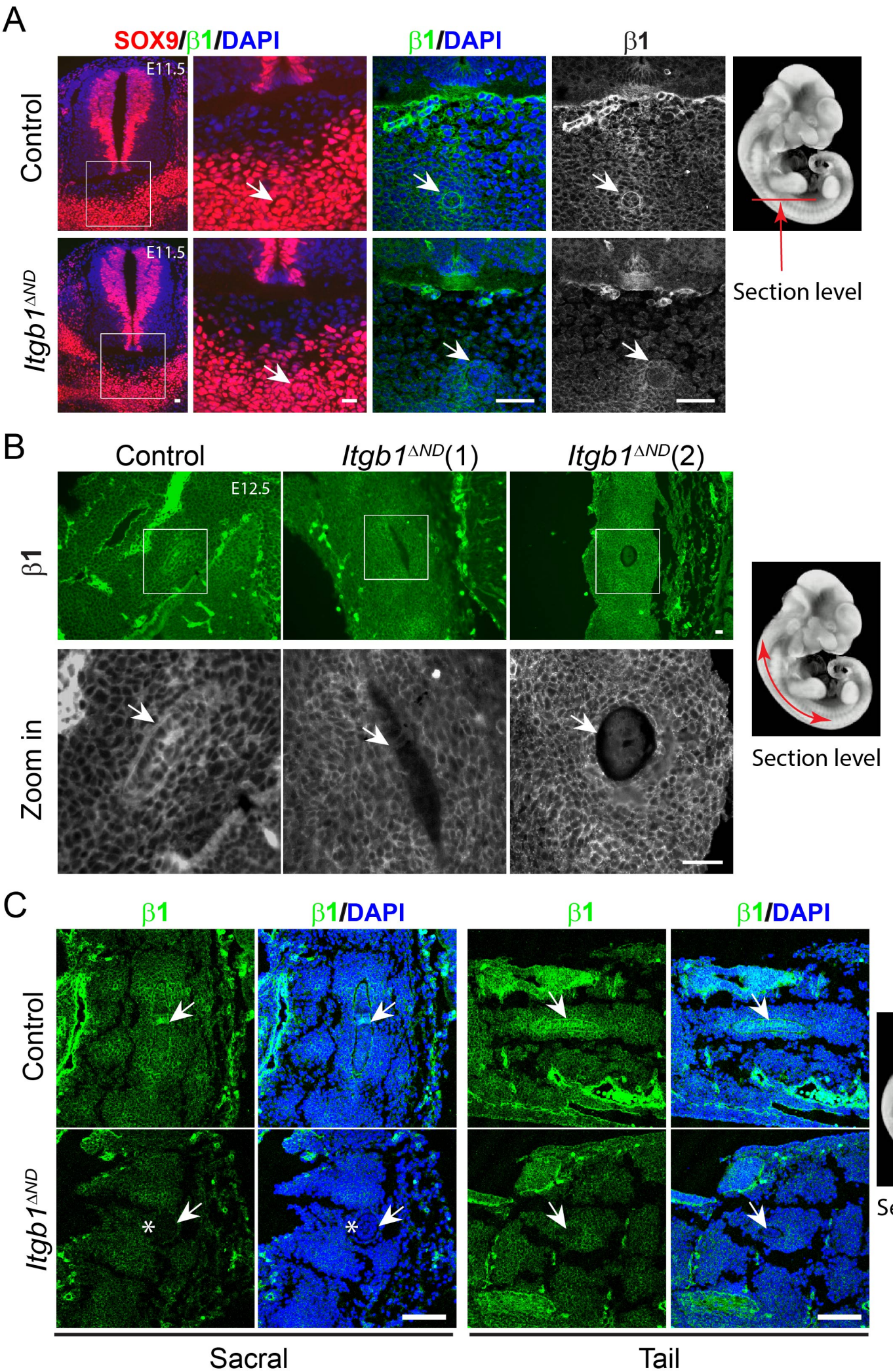

Figure S3: Specific ablation of β1 integrin expression from the mutant notochordal remnants. (A) Immunostaining against SOX9 (red), β1 integrin (green) and DAPI (blue) in the transverse sections from E11.5 embryos. Arrows: notochord. Noted that β1 integrin expression is significantly reduced comparing to the surrounding SOX9+ cells. (B-C) Immunostaining against β1 integrin (green) in the sagittal sections from E12.5 embryos. Noted that β1 integrin expression is specifically absent or reduced in the notochord descendants (arrows in B). (C) In the more posterior levels, such as sacral and tail vertebrae, β1 integrin expression is also slightly decreased in the regions surrounding the notochord. Arrows: notochord remnants. *: Note that the mutant notochord remnant was displaced to the lateral side. Scale bars: 50 μm for (A-B) and 100 μm for (C).

Figure S4

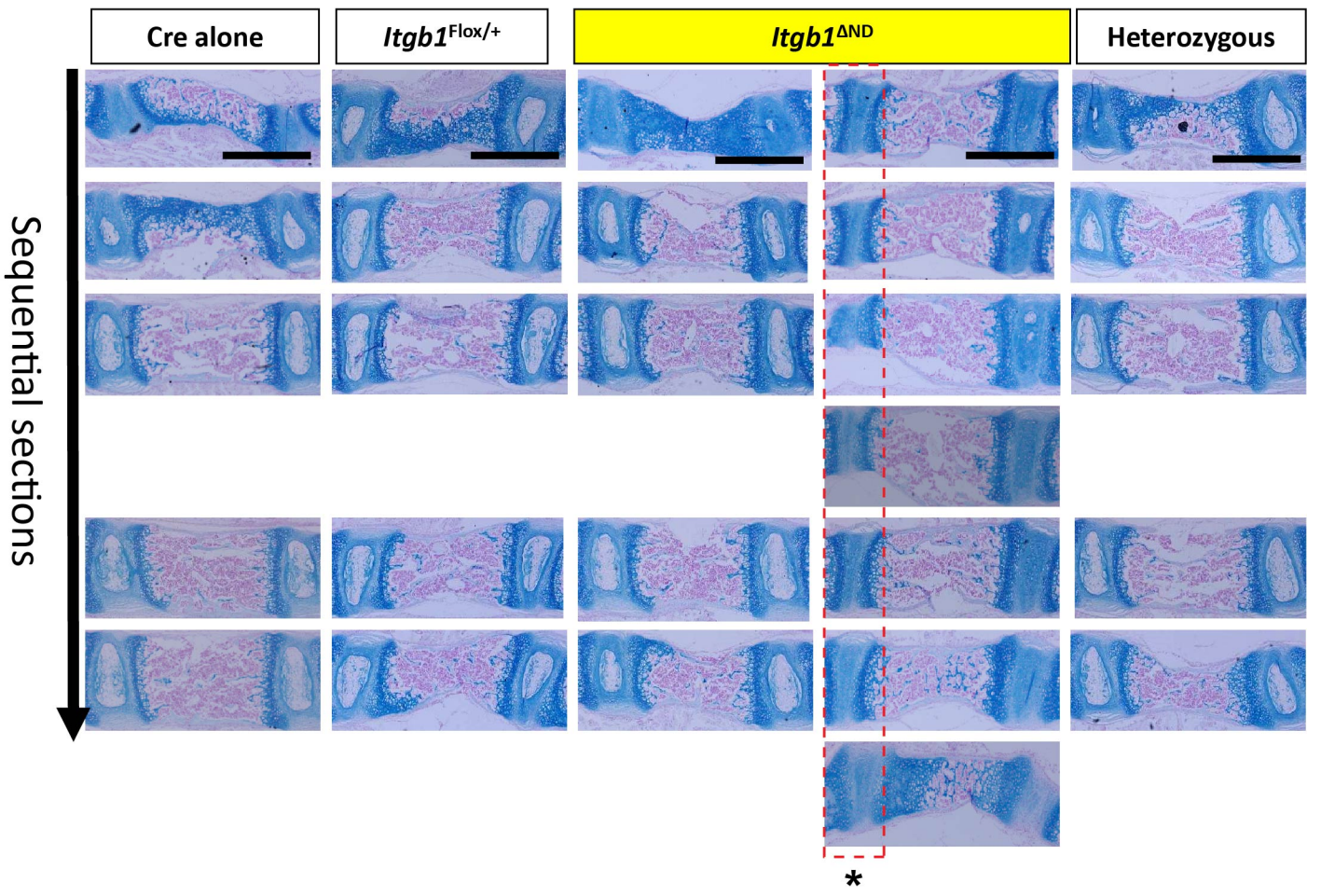

Figure S4: Histological analysis of the NP formation at postnatal stage (P10). Sequential sections were stained at every 5th section from the litter mates. *: Note that NP is not observed in all sections examined in the IVD highlighted in red. Scale bars: 200 µm.

Figure S5

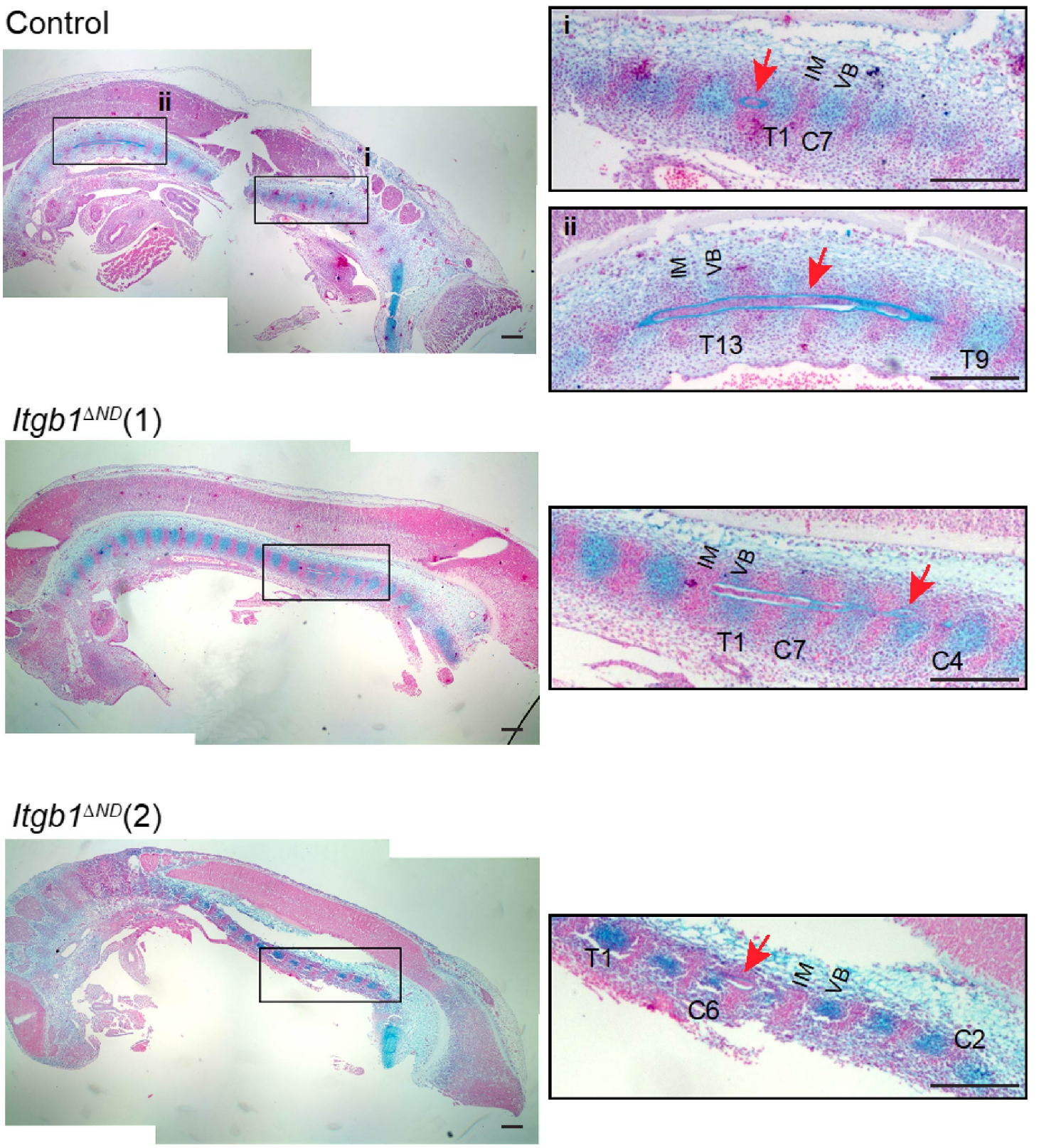

Figure S5: Histological analysis of the notochord remnants formation at E12.5. Note that notochord remnants (red arrows) are always centrally localized in control at different levels (i and ii) but are displaced from the midline in mutants. IM: intervertebral mesenchyme; VB: pre-vertebral region. Scale bars: 200 µm.

Figure S6

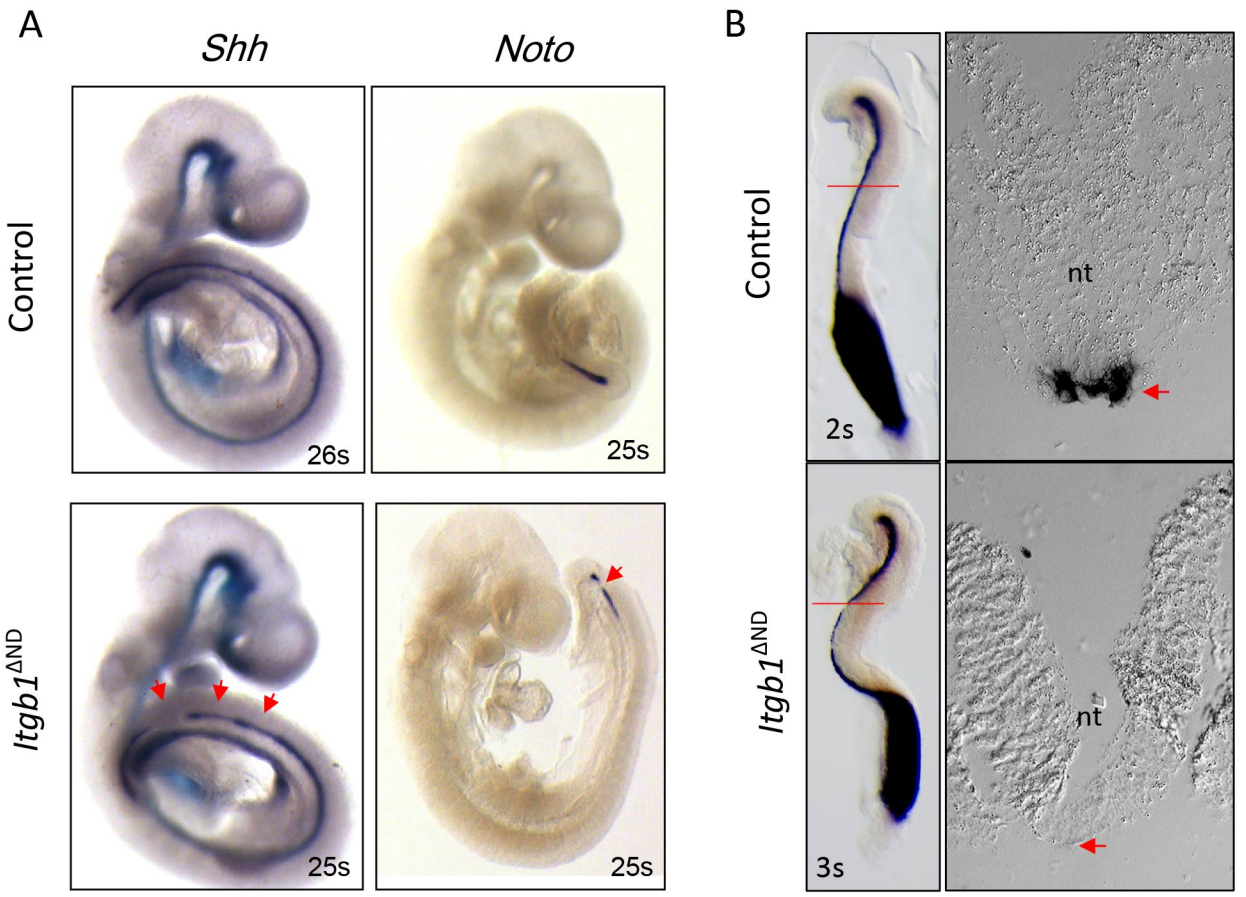

Figure S6: The notochord is interrupted in the *Itgb1*$^{\Delta ND}$ mutants. (A) *WISH* of *Shh* and *Noto* in the E9.5 embryos. Red arrows: interrupted gaps. (B) Detailed section analysis on the E8.5 embryos after *WISH* with *T* riboprobe. Red lines: section level. Red arrows: notochord. (C) Immunostaining against T (green) on the cross sections from embryos at E9.5. Nuclei are counter stained with DAPI. White arrows: notochord. (D) Immunostaining against SHH (green), NKX2.2, PAX6 or PAX7 (red) on the cross sections from embryos at E11.5. Arrows: notochord. Arrow heads: floor plate. nt: neural tube. da: dorsal aorta. Embryo stages are indicated with somite numbers. nt: neural tube. Scale bars: 50 μm.

Figure S7

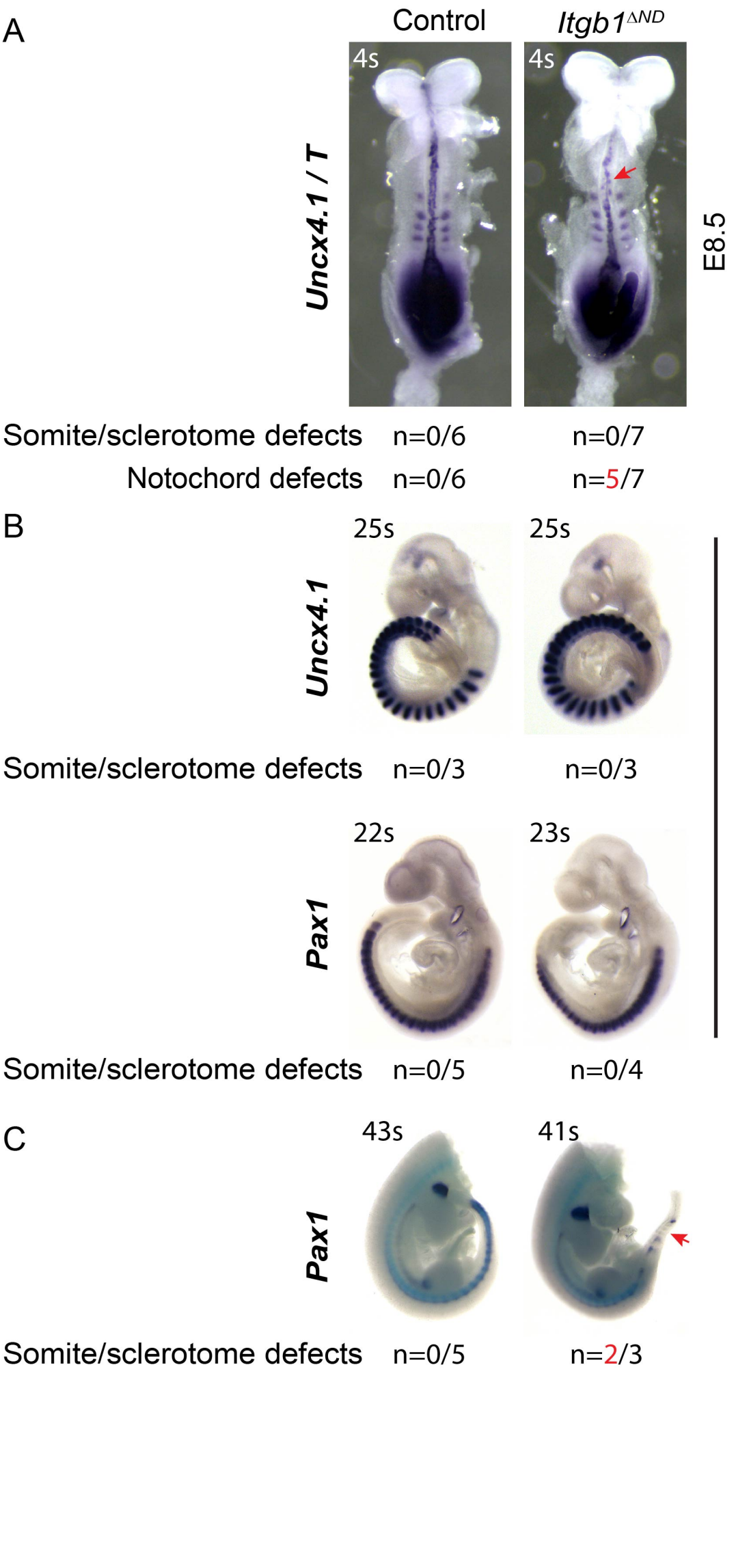

Figure S7: Sclerotome cell differentiation is defective in the *Itgb1*$^{\Delta ND}$ mutants from E10.5. (A-C) *WISH* of *Uncx4.1*, *T* and *Pax1* in the embryos at E8.5 (A), E9.5 (B) and E10.5 (C). n=number with defects/total number examined. Embryo age was indicated with somite numbers.

Figure S8

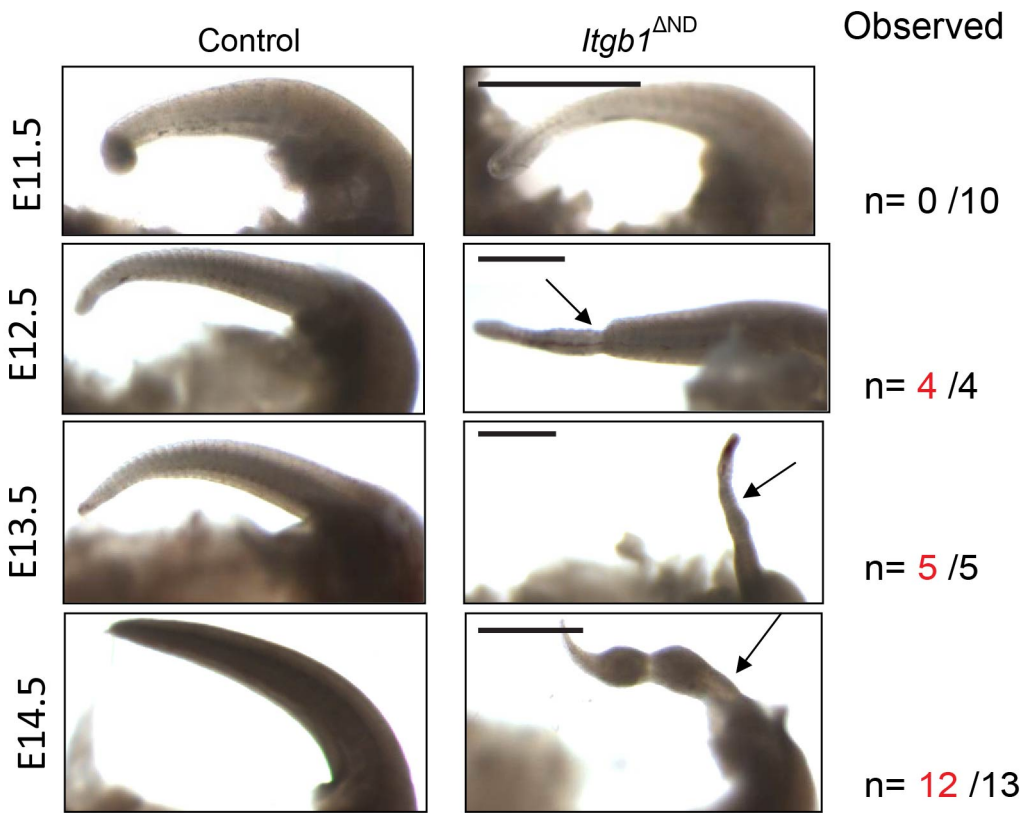

Figure S8: Tail morphology at different embryonic stages. n=number with defects/total number examined. Arrows: tail abnormalities. Scale bars: 1mm.

Figure S9

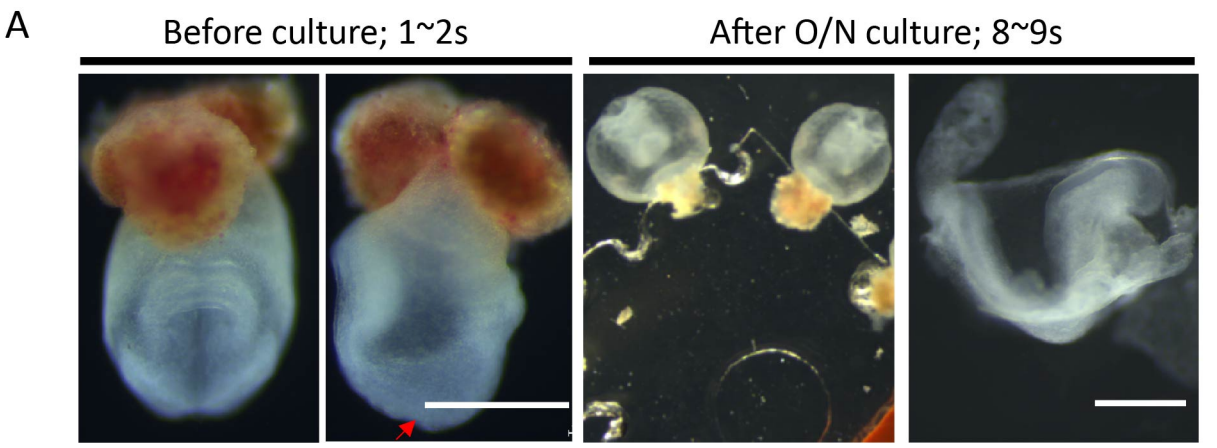

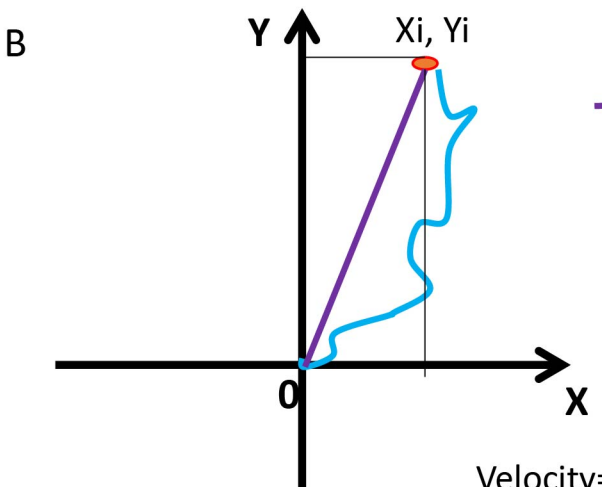

Euclidean (Euc) distance

Accumulated (Acc) distance

Cell end point

Velocity= changed accumulated distance / time;
Directionality = Euc / Acc distance;
Directionality ~1 → more persistent cell movement;
Directionality ~0 → less persistent cell movement.

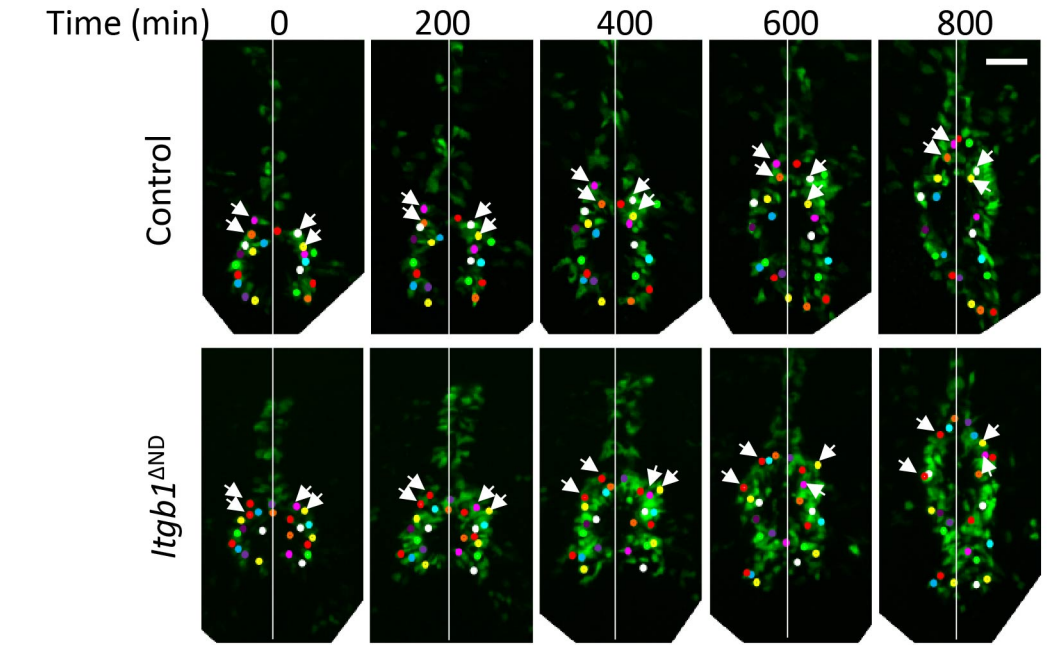

Figure S9: Embryo culture set up. (A) Embryos set up for time-lapse live imaging. Early head fold (EHF) stage (1~2s) embryo, shown before culture (frontal and lateral view). Embryos were then attached to the hand-made sticky edges and developed to 8~9s after ~17 hours culture and imaging. Red arrow indicates the position for O/N imaging. (B) Definitions of the parameters analyzed were illustrated. (C) Snapshot images of time-lapse movies. Cells tracked are indicated with color dotes. The cells highlighted with white arrows in the junction between the notochordal plate and the node were undergoing active convergent extension to the midline axis in the control embryo. This movement was less efficient in the *Itgb1*$^{\Delta ND}$ mutant embryo. A representative repeat was shown from 3 independent repeats (n=3 for each genotype). Scale bars: 500 μm for (A), 100 μm for (B).

Figure S10

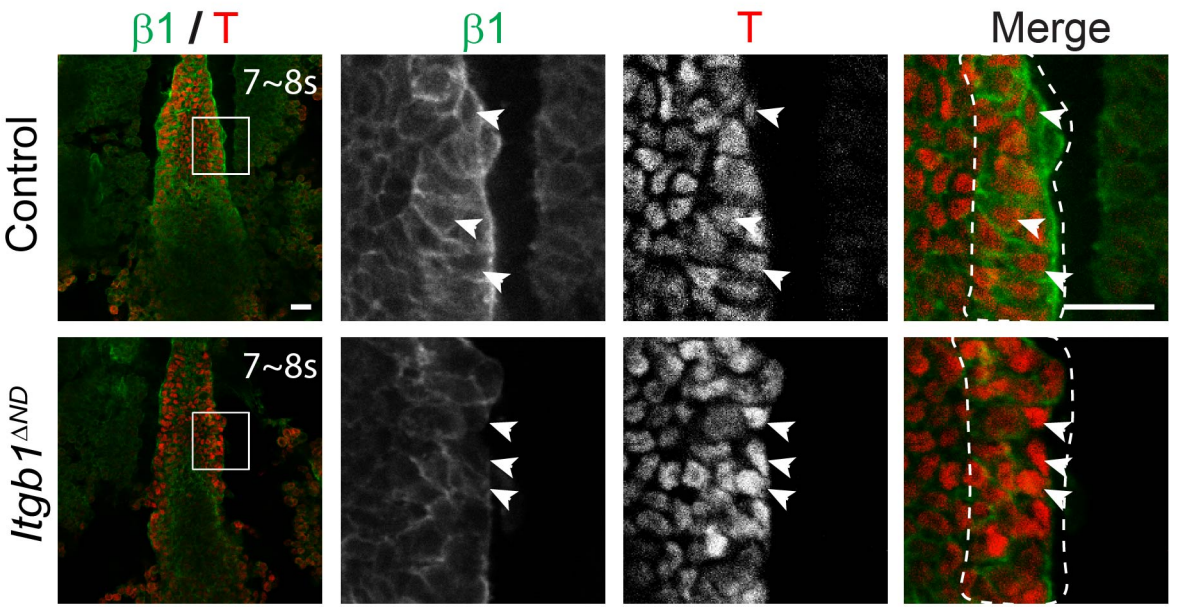

Figure S10: Reduction of β1 integrin expression in the mutant crown cells. Immunostaining against T (red) and β1 integrin (green) on the node region. Crown cells at the peripheral of the node were shown in higher magnification. Scale bars: 20 μm.

Figure S11

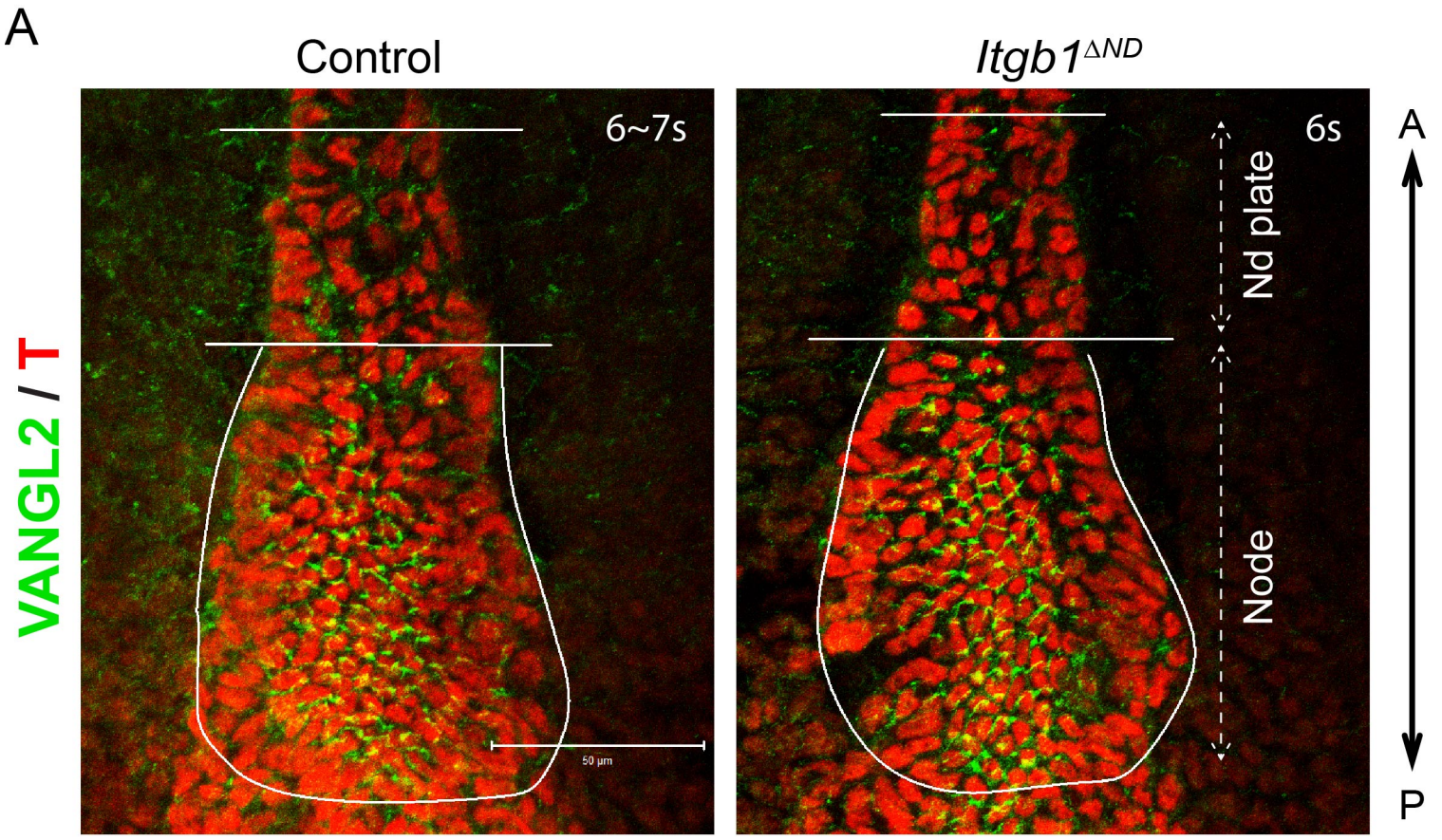

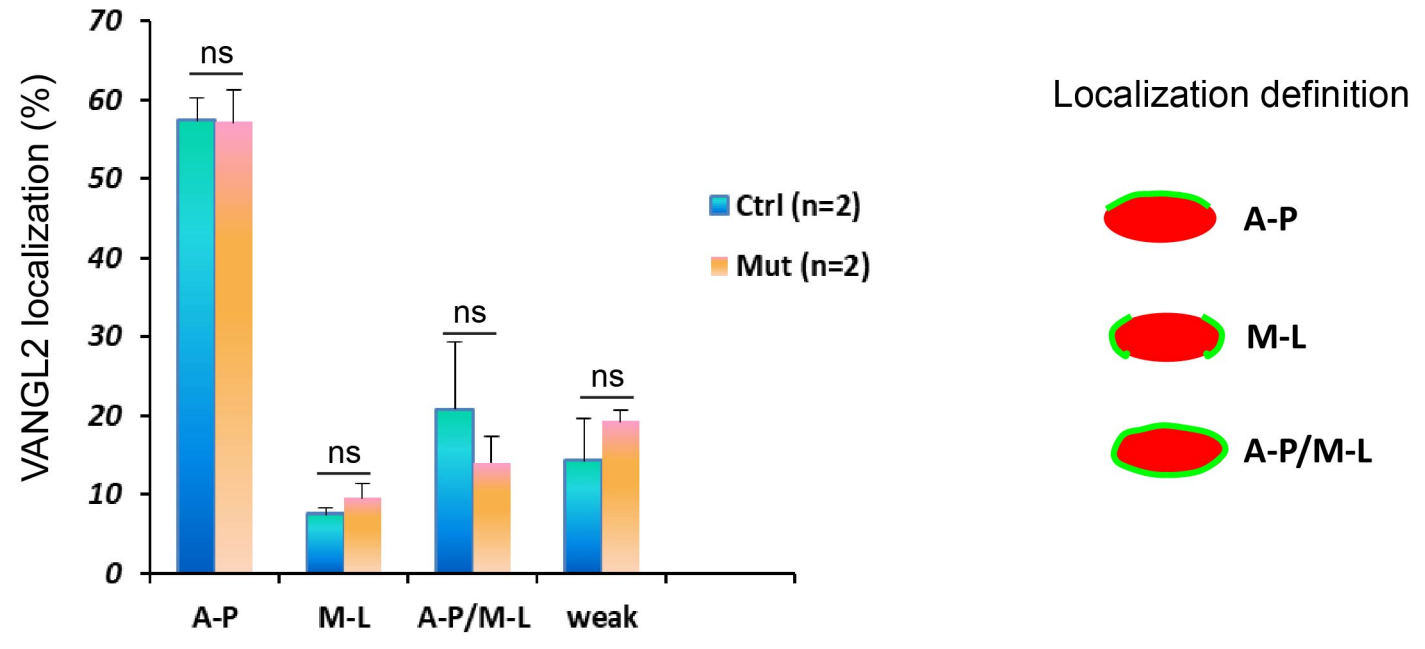

Figure S11: VANGL2 asymmetric localization analysis. (A) Whole embryo staining with T (red) and VANGL2 (green). VANGL2 localization within the node was analyzed and quantified. A-P: anterior-posterior axis. (B) Statistical graphs showing the percentage of the localizations are the data of mean±S.D from 2 pairs of control and mutants (two-tailed student t-test). A-P: anterior-posterior localized localized; M-L: medial-lateral localized; A-P/M-L: both directions; weak: weak signals. Scale bar: 50 μm.

Figure S12

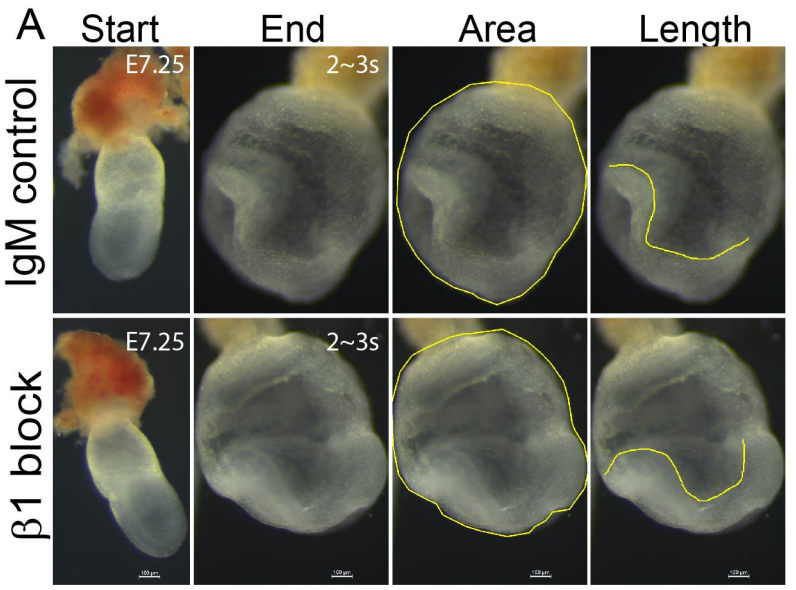

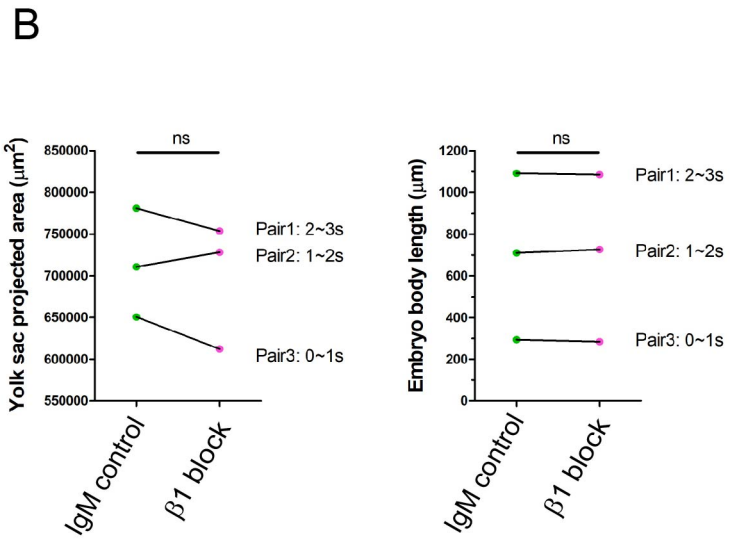

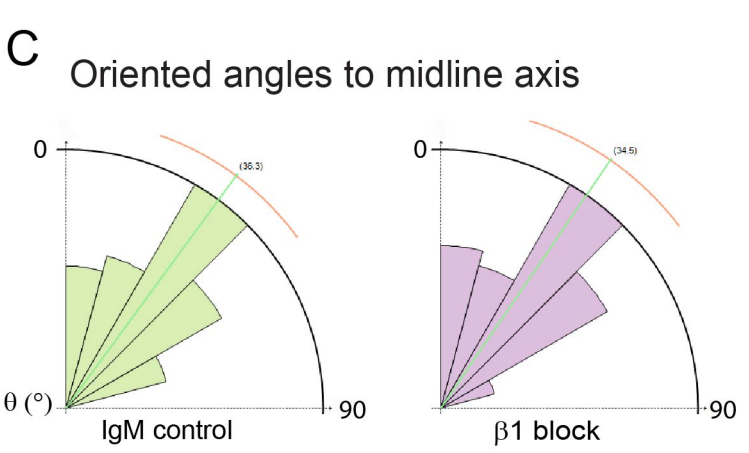

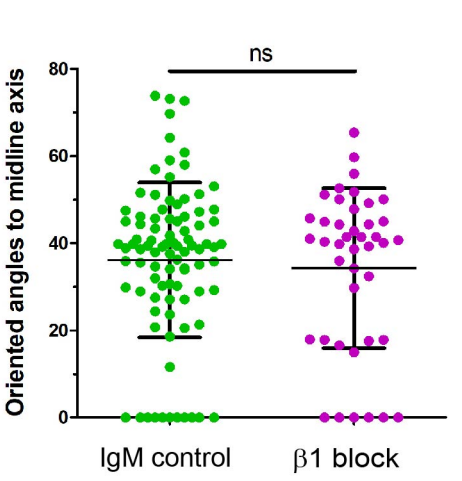

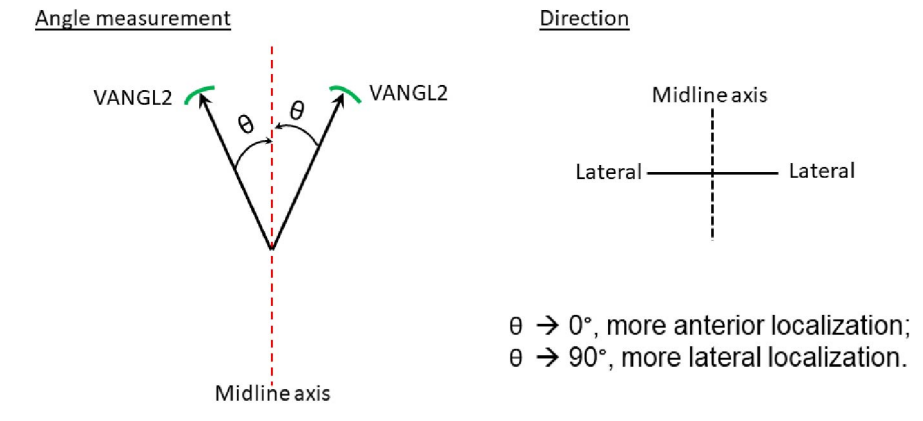

Figure S12: Embryo culture with blocking antibodies. (A) Embryo morphology before and after ~24 hours rotating culture in the presence of either IgM control or β1 specific functional blocking antibody. Age at the starting point and at the end point were indicated. The corresponding region and the embryo length applied for quantification are highlighted with yellow lines. Image shown is one representative from 3 independent repeats. (B) No difference of the projected yolk sac area and the embryo length at the end of culture. Statistical graphs are plotted in a paired manner. ns: no significance (paired student t-test). (C) VANGL2 orientation with respect to midline axis were measured and plotted in ROSE diagram. Quantification for all 3 pairs shown in (D). ns: no significance (two-tailed student t-test). (E) The orientations of the asymmetric VANGL2 signals to the embryo midline axis were measured and expressed with the angles from 0 to 90 degree. Scale bars: 100 μm.

Figure S13

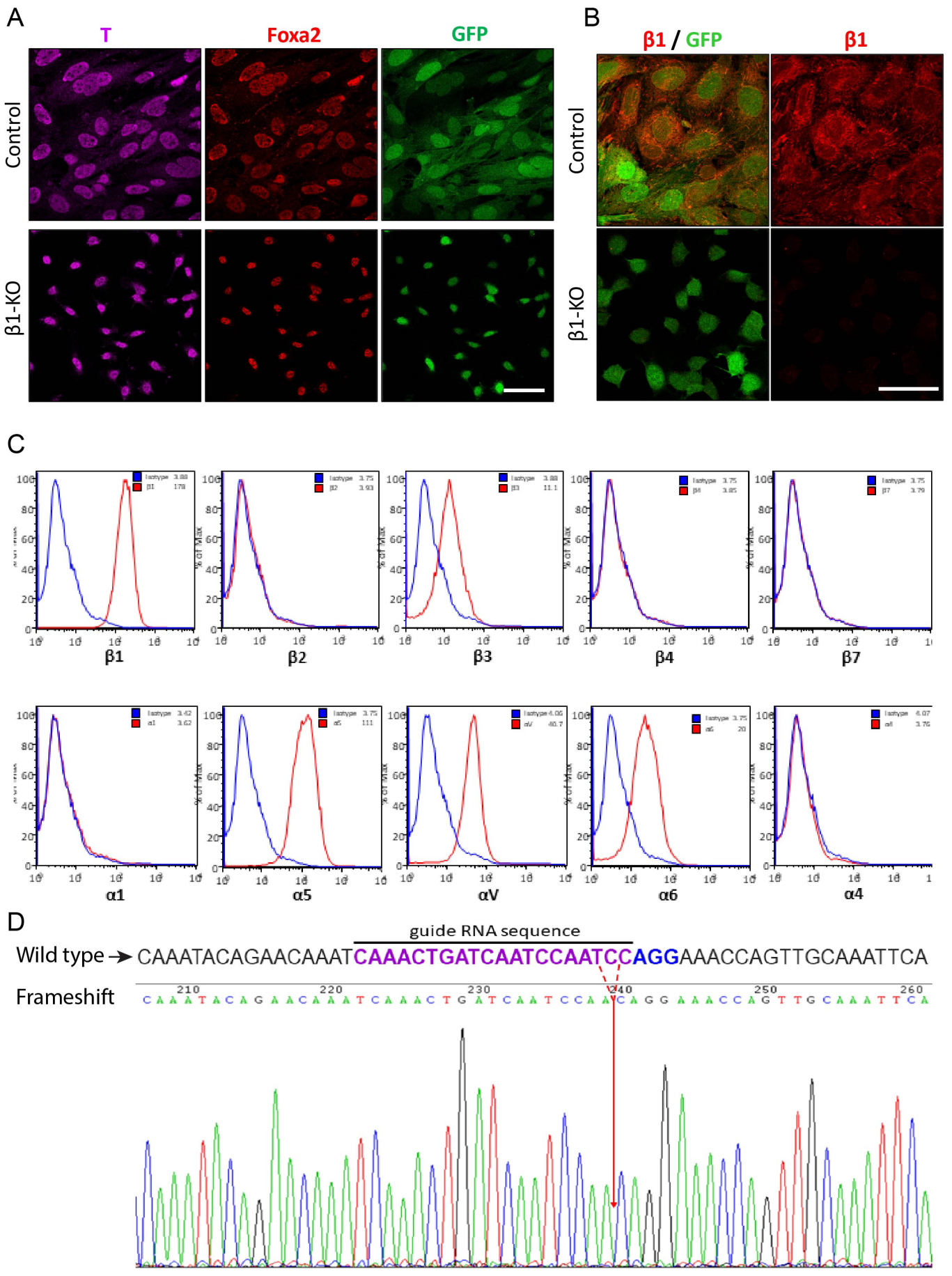

Figure S13: Generation and characterisation of the β1-KO notochordal cells. (A) The sorted notochordal cells immortalized by SV40 were stained with Foxa2 (red) and T (green). (B) *β1* integrin gene knockout was verified by immunofluorescence with β1 integrin antibody (red). GFP signals marking the notochordal cell lineages. (C) Integrin expression profile analysis in the immortalized notochordal cells. Isotype control shown in blue and integrin levels shown in red. (D) *β1* integrin gene knockout was verified by sequencing the frameshift. Red arrow indicates the 2 nucleotides (TC) deletion in the knockout cells. Guide RNA sequence and PAM sequence shown in magenta and blue, respectively. Scale bars: 50 μm.

Table S1

Random distribution of absent NP in mutant intervertebral discs

Genotype												
Control	S-N.	S-30	S-35	S-40	S-45	S-50						**Summary**
	T1	Y	0	0	0	0						Y
	T2	Y	Y	Y	Y	0						Y
	T3	Y	Y	Y	Y	0						Y
	T4	Y	Y	Y	Y	Y						Y
	T5	0	Y	Y	Y	Y						Y
	T6	0	0	Y	Y	Y						Y
	T7	0	0	Y	Y	Y						Y
	T8	0	0	Y	Y	Y						Y
	T9	Y	Y	Y	Y	Y						Y
	T10	Y	Y	Y	Y	Y						Y
	T11	Y	Y	Y	Y	Y						Y
	T12	Y	Y	Y	Y	Y						Y
	T13	N/A	N/A	N/A	N/A	N/A						N/A
Mutant-1	S-N.	S-5	S-10	S-15	S-20	S-25	S-30	S-35	S-40	S-45	S-50	S-55	**Summary**
	T1	0	0	0	Y	0	0	0	0	0	0	0	Y
	T2	0	0	0	0	Y	Y	Y	0	0	0	0	Y
	T3	0	0	0	0	0	0	Y	0	0	0	0	Y
	T4	0	0	0	0	0	0	0	0	0	0	0	0
	T5	0	0	0	0	0	0	0	0	0	0	0	0
	T6	0	0	0	0	0	0	0	0	0	0	0	0
	T7	0	0	0	0	0	0	0	0	0	0	0	0
	T8	0	0	0	0	0	0	0	0	0	Y	0	Y
	T9	0	0	0	0	0	0	0	0	0	0	0	0
	T10	0	0	0	0	0	0	0	0	0	0	0	0
	T11	0	0	0	0	0	0	0	0	0	0	0	0
	T12	0	0	0	0	0	0	0	0	0	0	0	0
	T13	0	0	0	0	0	0	0	0	0	0	0	0
Mutant-2	S-N.	S-5	S-10	S-15	S-20	S-25	S-30	S-35	S-40	S-45	S-50	S-55	**Summary**
	T1	0	0	0	0	0	0	0	0	0	0	0	0
	T2	0	0	0	0	0	0	0	0	0	0	0	0
	T3	0	0	0	0	Y	0	Y	0	0	0	0	Y
	T4	0	0	0	0	Y	0	Y	0	0	0	0	Y
	T5	0	0	0	0	0	Y	Y	Y	Y	Y	0	Y
	T6	0	0	0	0	0	0	0	0	0	0	0	0
	T7	0	0	0	0	0	0	0	0	0	0	0	0
	T8	0	0	0	Y	Y	Y	Y	Y	0	0	0	Y
	T9	0	0	0	0	0	0	0	0	0	0	0	0
	T10	0	0	0	0	0	0	0	0	0	0	0	0
	T11	0	0	0	0	0	0	0	0	0	0	0	0
	T12	0	0	Y	Y	Y	0	0	0	0	0	0	Y
	T13	0	0	0	0	0	0	0	0	0	0	0	0

S-N.: section ID number; T1-T13: the corresponding thoracic levels;
0: NP not found; Y: NP found
N/A: the level was not included in the sections.

Table S2

Phenotype penetrance at different embryonic stages

Mutant Stage	E8.0-E8.5	E8.5	E8.75-E9.5		E10.5
Method	WISH	DoubleWISH	WISH	WIHC	WISH
Analyzed	12	7	5	8	5
Interrupted	8	5	4	4	5
Overall penetrance of interrupted notochord: 26/37= ~70% (wt: 1/49=2%)					
Mutant (Section IFC)	Stage	~E9.0 14-17s	E9.25 18-21s	E9.5 22-25s	
	Analyzed	5	5	6	
	D-V defects	1	4	0	
Penetrance of notochord D-V displacement from midline: 5/16=~31% (wt: 1/21=4.7%)					
Mutant (Section IFC)	Stage	~E9.0 14-17s	E9.25 18-21s	E9.5 22-25s	E8.75-E9.5 WIHC
	Analyzed	5	5	6	8
	L-R defects	2	0	2	2
Penetrance of notochord L-R displacement from midline: 6/24=~25% (wt: 1/28=3.6%)					

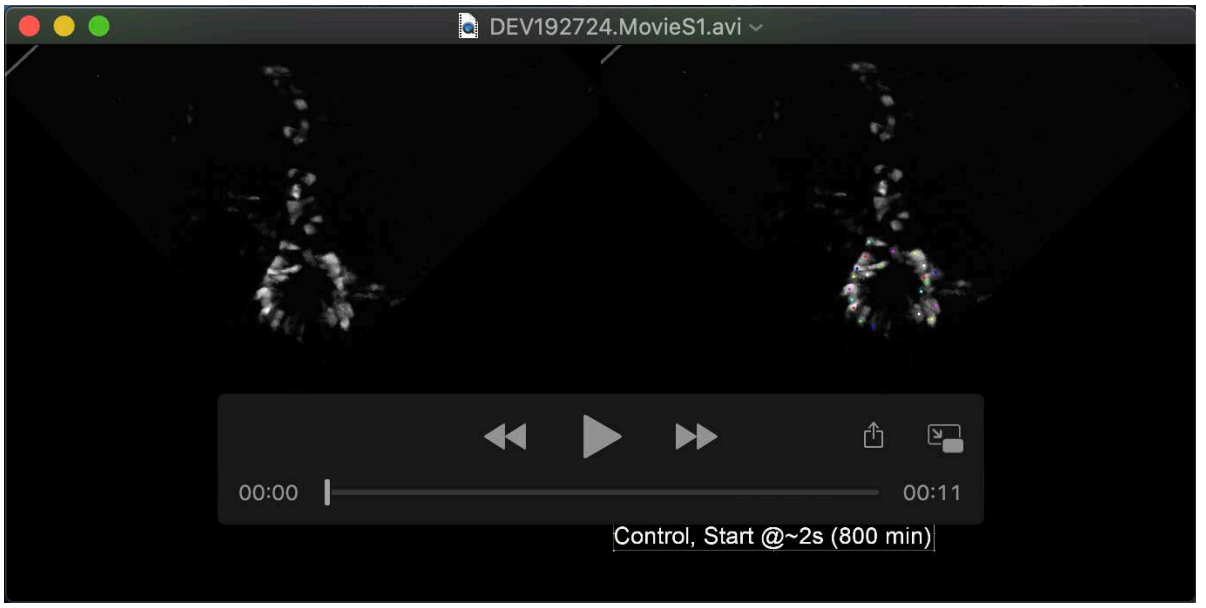

Movie 1: Representative time-lapse movie of the node and notochordal cell movement in control embryo (*Foxa2mNE-Cre* X zEG). Left: original movie; Right: overlaid with cell trajectory. Frames were captured every 10 minutes. Repeats n =3.

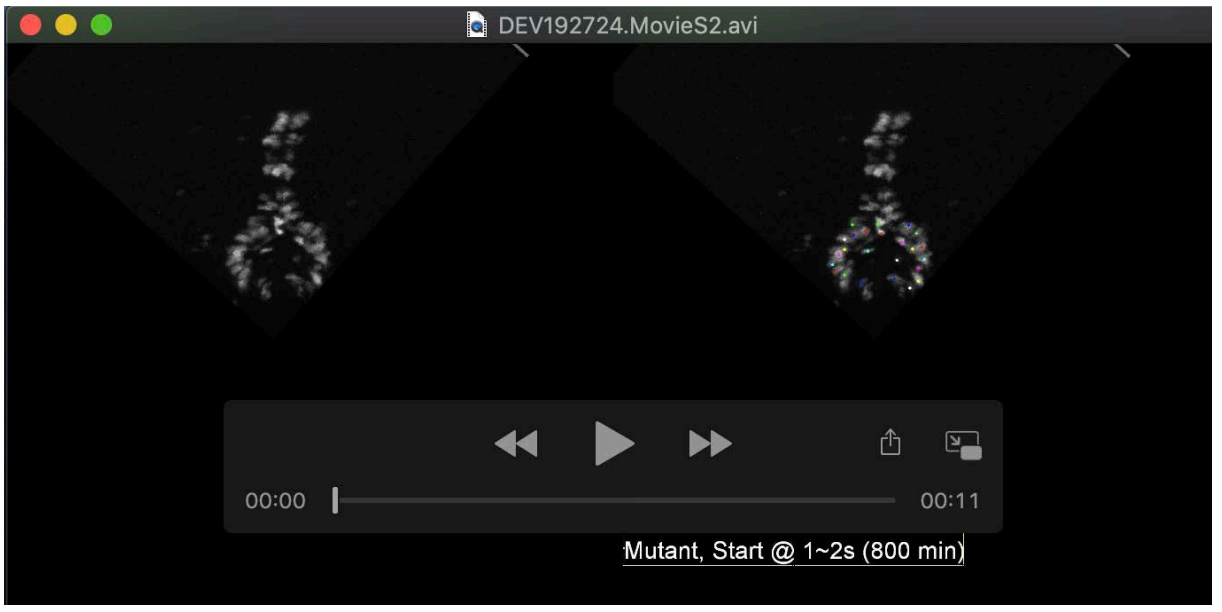

Movie 2: Representative time-lapse movie of the node and notochordal cell movement in mutant embryo (*Itgb1*$^{\Delta ND}$ X zEG). Left: original movie; Right: overlaid with cell trajectory. Frames were captured every 10 minutes. Repeats n =3.